Geophysical Fluid Dynamics. 1970. Vol. 1, pp. 303–355

Internal Gravity Waves in Atmospheres with Realistic Dissipation and Temperature Part I. Mathematical Development and Propagation of Waves into the Thermosphere

RICHARD S. LINDZEN

Department of Geophysical Sciences
University of Chicago

Received November 13, 1969

Abstract—In this, the first part of a three part study, we develop a model for the theoretical analysis of 3-dimensional internal gravity waves in atmospheres with arbitrary distributions of basic temperature, molecular weight, viscosity and conductivity (both eddy and molecular), Newtonian cooling, anisotropic hydromagnetic (ion) drag, and thermal excitation. Attention is given to the physical bases for our models, and a detailed outline is given of the numerical method used to solve the resulting system of equations.

As an application of the above development, we study the ability of five particular gravity waves (chosen for their observed importance in the neighborhood of 90–100 km—four of the waves are simulated tidal modes) to propagate from 90 km into the thermosphere. We choose to define the thermosphere as that portion of the atmosphere above the turbopause (*ca.* 110 km). Among the most significant results to emerge are the following: (i) the effects of molecular viscosity and conductivity appear to be more significant than the effects of hydromagnetic drag, and (ii) while most waves considered are significantly attenuated somewhere between 90 km and the thermosphere, the main semidiurnal tidal mode is not. In fact, semidiurnal temperature oscillations of only a few degrees amplitude at 90 km can give rise to oscillations of over a hundred degrees amplitude in the exosphere.

1. Introduction

Given that atmospheric tides and thermal tides are simply special cases of internal gravity waves, then it becomes fair to say that the largest part of the dynamics of the atmosphere above 90 km is described by internal gravity waves.[8,10,32] Their importance in the mesosphere,[30] stratosphere[35] and troposphere[27] is also likely to

be considerable. The theory of such waves in inviscid, non-conducting atmospheres without ion drag is straightforward[9,20] and reasonably successful in describing observations outside the earth's surface boundary layer and below about 95 km. Unfortunately, within the surface boundary layer, and, more important, above 95 km the effects of viscosity and conductivity assume great importance. Moreover, in the upper atmosphere hydromagnetic drag is, *a priori*, likely to be of considerable importance. However, its role is complicated by the fact that it is anisotropic; i.e., the drag on westerly winds can be different from the drag on southerly winds.[2,11,17,23] The effects of Newtonian cooling and variable basic temperature have been evaluated for inviscid atmospheres.[20] We shall show that the effects of the latter can be more profound in a viscous atmosphere.

There are now in the literature several attempts to study gravity waves in a viscous, thermally conducting atmosphere where both these processes are permitted to increase in importance inversely with density: most notably Pitteway and Hines,[29] and Midgely and Liemohn.[24] In these studies the atmosphere was approximated by a finite number of homogeneous layers in each of which analytic solutions are possible. Continuity, boundedness, and/or radiation-type conditions are used to match solutions across layer interfaces. These studies give valuable results on the dissipative effects of viscosity and conductivity, and their relative simplicity have permitted the presentation of results for general choices of frequency and horizontal wavenumber. However, they are not sufficiently accurate to permit a quantitatively accurate determination of the reflectivity resulting from the variation with height of viscosity and thermal conductivity. Relatedly, they do not readily lend themselves to the accurate calculation of the continuation of waves in the lower atmosphere into the upper thermosphere. Moreover, the convergence properties of layer methods were not clear at the time of these studies. For inviscid adiabatic atmospheres Pierce (1966) proved convergence in the limit of infinitesimal layers; Vincent[33] showed that more than 10 layers per vertical wavelength are needed. For this resolution finite-difference methods are simpler. It should be added that Pitteway and Hines[29] considered only isothermal atmospheres, and Midgely and Liemohn[24] omitted ion drag. In addition to these studies, Volland (1969) has used layer methods to examine waves in an atmosphere with thermal conductivity but without viscosity. He maintained (incorrectly as we shall see) that ion drag would dominate the momentum balance. Finally, mention must be made of Yanowitch's[36] analytic investigation of the behavior of internal gravity waves in an isothermal atmosphere with viscosity but no conductivity. Although his model was physically incomplete, it clearly and accurately demonstrated the ability of variable viscosity to reflect waves.

In the present study we develop the equations for linearized three dimensional internal gravity waves in an atmosphere with arbitrary distributions of basic temperature, molecular weight, conductivity, viscosity, Newtonian cooling, anisotropic ion drag and thermal excitation. Due to the anisotropic ion drag the resulting set of equations forms on eighth order system (as opposed to the sixth order system considered by Midgely and Liemohn.[24] In principle we may rewrite these equations in finite difference form; the finite difference system can be solved; and the solution to the finite difference system can be brought arbitrarily close to the exact solution by reducing the mesh interval. In fact many common finite difference methods like the Runge–Kutta method require inordinate computational accuracy because of the exponential nature of some of the solutions when viscosity and conductivity are present,[1,24] and thus become unusable. However, a technique described by Lindzen and Kuo[22] avoids such problems and makes the finite difference solution of the equations easy and computationally rapid in practice as well as principle. Grid intervals smaller than 20 m are easily handled.

We have used the above mentioned method to solve our equations for a large number of physical configurations. We find, not surprisingly, that the effect of any given process depends not only on the frequency and horizontal wavenumbers of the wave under consideration, but on the distribution of the process and on the magnitude and distribution of other processes. Moreover, the effects often consist in several changes in the vertical structure which are not readily describable in terms of a few parameters. Thus, the compact presentation of our results becomes virtually impossible. Philosophically, we are almost forced to conclude that our solution is

defined not by an equation or a graph but by a computer program (which is not really impractical since a given case can be run in well under a minute on a fast computer). Our situation is, in practice, not quite so extreme since of all the gravity waves that must be present in the atmosphere only a small number of modes appear to account for most of the wind amplitude in the upper atmosphere, at least between 80 and 110 km[32]: namely, the first two propagating, symmetric, migrating solar semidiurnal tidal modes, the first propagating and the first trapped symmetric, migrating solar diurnal tidal modes and a mode of unknown origin with a period of about 3 hours and a vertical wavelength on the order of 20 km. (For a detailed description of tidal modes see Lindzen and Chapman.[20]) Thus, we may at least hope to learn a great deal about upper atmosphere dynamics by studying a relatively small number of modes rather than a continuous distribution of frequencies and horizontal wave numbers. Moreover, in studying tidal modes we may reasonably expect to learn more about tides at all levels. As is well known, the structure of tidal modes is significantly influenced by the rotation and curvature of the earth. However, it is also true that in the absence of viscosity and any form of Rayleigh friction (like ion drag), the vertical structure of a tidal mode is identical to that of an internal gravity wave in a plane, non-rotating atmosphere, whose period is equal to that of the tidal mode, and whose wavelength in one of the horizontal directions is equal to the zonal wavelength (i.e., wavelength in the east-west direction) of the tidal mode at the equator—provided that the wavenumber of the gravity wave in the remaining horizontal direction is properly chosen according to a simple procedure to be described in Sec. 21. Moreover, at the equator where the vertical component of the earth's rotation vector is zero, the physics of the two waves is identical, and indeed the two waves are close approximations to each other. In the absence of viscosity and Rayleigh friction (Newtonian cooling and conductivity may remain; see Dickinson and Geller[4]) a study of the " equivalent " gravity wave tells us exactly what happens to the tidal mode. In more complicated cases we expect that study of the " equivalent " gravity wave will be indicative of the vertical variations of the tidal mode—especially in the neighborhood of the equator. The problem of correspondence results from the fact that in the presence of rotation

the tidal equations, including friction, are no longer separable in their height and latitude dependence. Crudely stated, the latitude structure of a tidal mode will change with height in the presence of friction. For semi-diurnal modes, where the effect of rotation is not overwhelming, this effect seems unlikely to be of great importance. For diurnal modes whose latitude structure is importantly influenced by rotation, the effect is likely to be of greater importance—at least away from the equator at heights where friction is very important. Nevertheless, in the present investigation, we restrict our consideration of tides to the study of " equivalent " internal gravity waves.

For convenience we have divided the presentation of our results into three parts. In this, the first part, we introduce our equations, describe our models for various processes and for the basic state, and describe our numerical method and its convergence properties. Our actual computations will be for the five modes mentioned earlier: a 2-dimensional mode with a period of 3 hr and a typical adiabatic vertical wavelength of 20 km, and four 3-dimensional " equivalent " gravity waves for the first two symmetric vertically propagating migrating semidiurnal, the first symmetric vertically propagating migrating diurnal and the first symmetric vertically trapped migrating diurnal tidal modes. In Part I we study the ability of these modes to penetrate into the thermosphere from below 90 km. Solutions with and without variable temperature, viscosity and conductivity, and ion drag are compared. Most important, we show how the transition from essentially inviscid solutions below 100 km to rigid body motion (where both horizontal velocity and temperature oscillations are independent of altitude) occurs for each mode. This transition occurs because molecular diffusivities increase inversely with the mean density. Indeed, it will be shown that molecular viscosity and conductivity dominate all other processes, including ion drag, above about 200 km.

In Part II we quantitatively consider the solar tides as excited by insolation absorption by ozone in the mesosphere and water vapor in the troposphere. We also reexamine the effect of surface temperature oscillations in exciting tides. Quantitative results are made possible by establishing, in detail, the correspondences between the tidal modes and the " equivalent " gravity waves. We consider the effects of viscosity (including different eddy viscosities and surface

drag coefficients), Newtonian cooling and variable temperature on the amplitudes and phases of thermal tides between the ground and the ionosphere. We are able to extend an earlier theory of the turbopause[18] in order to explain the sharp cessation of turbulence at the turbopause. We are also able to show that a proper inclusion of the surface boundary layer does *not* correct the discrepancy between the observed phase of the semidiurnal surface pressure oscillation and that predicted for excitation by H_2O and O_3 heating.

In Part III we study, in detail, the tides of the thermosphere—both those propagated from below and those excited *in situ* through absorption of ultraviolet radiation by O_2 and through EUV absorption. Since the problem of non-separability is likely to be important here, we examine the effect of assuming different latitude structures. Our results show that only a negligible portion of the diurnal oscillation is excited below—most is excited *in situ*. We show that the efficiency of a given *in situ* excitation depends very much on the mean temperature distribution of the thermosphere. More important, we find that the semi-diurnal tide excited in the mesophere and troposphere is as important (or more important) in the thermosphere as the diurnal oscillations excited *in situ*.

2. Equations

Our equations are, for the most part, the Navier–Stokes equations for a plane, nonrotating atmosphere, where the most important approximations are the replacement of the vertical momentum equation by the hydrostatic pressure relation, and the use of the perfect gas law (the molecular weight, however, is not taken to be constant). Both approximations are usual and adequate for the cases under study. In addition, ion drag, radiative cooling and heating are allowed for. The equations follow:

$$\frac{\mathrm{d}\rho}{\mathrm{d}t} + \rho \nabla \cdot \mathbf{v} = 0 \tag{1}$$

$$\rho \frac{\mathrm{d}u}{\mathrm{d}t} = -\frac{\partial p}{\partial x} + \mathscr{V}_x - \rho D_x u \tag{2}$$

$$\rho \frac{\mathrm{d}v}{\mathrm{d}t} = -\frac{\partial p}{\partial y} + \mathscr{V}_y - \rho D_y v \tag{3}$$

$$\frac{\partial p}{\partial z} = -\rho g \tag{4}$$

$$\rho c_v \frac{\mathrm{d}T}{\mathrm{d}t} = \rho J + \mathscr{K} + \frac{p}{\rho}\frac{\mathrm{d}\rho}{\mathrm{d}t} - \mathscr{C} \tag{5}$$

$$p = \rho R T \tag{6}$$

where x = distance in the horizontal direction to be associated with west-to-east

y = distance in the horizontal direction to be associated with south-to-north

z = distance upwards

t = time

p = pressure

ρ = density

T = temperature

u = velocity in the x-direction

v = velocity

g = acceleration by gravity = $9.8\ \mathrm{m\ sec^{-2}}$

c_v = heat capacity at constant volume

R = gas constant for air = $\tilde{R}/M$

$\tilde{R}$ = universal gas constant

M = mean molecular weight

$\mathscr{V}_i$ = Force in the i-direction due to eddy and molecular viscosity

D_i = coefficient for ion drag in the i-direction

$\mathscr{K}$ = Heating per unit mass per unit time due to eddy and molecular conductivity

$\mathscr{C}$ = Infrared cooling rate per unit mass

J = Radiative heating rate per unit mass

Also

$$\frac{\mathrm{d}}{\mathrm{d}t} = \frac{\partial}{\partial t} + u\frac{\partial}{\partial x} + v\frac{\partial}{\partial y} + w\frac{\partial}{\partial z} \tag{7}$$

where w = vertical velocity.

For future reference

c_p = heat capacity at constant pressure = $R + c_v$

and

$$\gamma = c_p/c_v .$$

$\mathscr{V}_i$, D_i, $\mathscr{K}$, $\mathscr{C}$ and J will be defined in the course of describing our model. M (and hence R) and γ will be allowed to vary with z. Gravitational acceleration, g, whose z-variation is less marked, will be held constant.

In this study we will consider linearized perturbations on a steady, stationary basic state, varying only with z.

2A. Basic State

The equations for the basic state are:

$$\frac{\partial p_0}{\partial z} = -\rho_0 g \tag{8}$$

$$\rho J + \mathscr{K} - \mathscr{C} = 0 \tag{9}$$

$$p_0 = \rho_0 R T_0 \tag{10}$$

The solution of (8)–(10) is in general a very complicated problem; namely, the solution of the equations for radiative-diffusive equilibrium. What is generally done in wave problems is to adopt a distribution $T_0(z)$ and assume that it represents an equilibrium solution, and then solve (8) and (10) for the appropriate distributions of $\rho_0(z)$ and $p_0(z)$. In order to do this, we must also adopt a distribution for $R(z)$.

Our solutions for p_0 and ρ_0 are

$$p_0 = p_0(0)\, \mathrm{e}^{-x} \dagger \tag{11}$$

$$\rho_0 = p_0/gH \tag{12}$$

where

$$x = \int_0^z \frac{\mathrm{d}z}{H} \tag{13}$$

and

$$H = \frac{RT_0}{g} \tag{14}$$

† Unfortunately, x in this paper is used for both the height in scale heights and the west–east coordinate. For the remainder of this paper x will refer to the height in scale heights unless otherwise noted. x_{ew} will be used for the west–east coordinate.

When R is a constant, H is proportional to T_0 and their derivatives are, within constant factors, interchangeable. Now it must be recalled that

$$\frac{\mathrm{d}T}{\mathrm{d}z} = \frac{g}{R}\frac{\mathrm{d}H}{\mathrm{d}z} - \frac{T}{R}\frac{\mathrm{d}R}{\mathrm{d}z} \tag{15}$$

z- and x-derivatives are simply related:

$$\frac{1}{H}\frac{\mathrm{d}}{\mathrm{d}x} = \frac{\mathrm{d}}{\mathrm{d}z} \tag{16}$$

In choosing T_0 we wanted a simple analytic expression which would give a smooth representation of varying atmospheres like the ARDC and EQUATORIAL STANDARD by simply changing a few parameters. Our choice of expression was based on the fact that the atmosphere consists in layers of relatively constant temperature gradient separated by extrema. Thus we may write

$$\frac{\mathrm{d}T_0}{\mathrm{d}z} = c_1 + \sum_{i=1}^{4} \left(\frac{c_{i+1} - c_i}{2}\right)\left(1 + \tanh\left(\frac{z - z_i}{\delta_i}\right)\right), \tag{17}$$

where δ_i is the half-thickness of a region centered approximately at z_i in which $\mathrm{d}T_0/\mathrm{d}z$ goes from c_i to c_{i+1}. (7) is easily integrated and differentiated to yield

$$T_0 = T_0(0) + \frac{c_1}{2} z + \sum_{i=1}^{4} \delta_i \left(\frac{c_{i+1} - c_i}{2}\right) \ln\left\{\frac{\cosh\,(z - z_i/\delta_i)}{\cosh\,(z_i/\delta_i)}\right\}, \tag{18}$$

$$\frac{\mathrm{d}^2 T_0}{\mathrm{d}z^2} = \sum_{i=1}^{4} \left(\frac{c_{i+1} - c_i}{2\delta_i}\right) \mathrm{sech}^2\left(\frac{z - z_i}{\delta_i}\right). \tag{19}$$

The variation in M (and hence R) results from the dissociation of O_2 and the diffusive separation of O_2 and N_2 from O in the region roughly between 200 km and 400 km; above 400 km O predominates. Thus, for M we write

$$M = 28.9 - 6.45\left(1 + \tanh\left(\frac{z - 300\ \mathrm{km}}{100\ \mathrm{km}}\right)\right) \tag{20}$$

This region also represents the transition from a diatomic gas where $\gamma = 1.4$ to a monotomic gas where $\gamma = 1.67$. Thus, for future reference we write:

$$\gamma = 1.4 + 0.135\left(1 + \tanh\left(\frac{z - 300\ \mathrm{km}}{100\ \mathrm{km}}\right)\right). \tag{21}$$

In Parts I and II we study the behavior of internal gravity waves in both an isothermal atmosphere and an atmosphere with a variable temperature distribution similar to the standard atmospheres and an exosphere temperature of 800 °K. For the latter

$c_1 = -6.5°/\text{km}$, $c_2 = 3.265°/\text{km}$, $c_3 = -5.14°/\text{km}$, $c_4 = 6.81°/\text{km}$, $c_5 = 0.0°/\text{km}$,

$z_1 = 16.0$ km, $z_2 = 50.0$ km, $z_3 = 82.0$ km, $z_4 = 180.0$ km,

$\delta_1 = 4.0$ km, $\delta_2 = 7.5$ km, $\delta_3 = 9.0$ km, and $\delta_4 = 20.0$ km.

Both temperature distributions are shown in Fig. 1. Also shown are the distributions of x with z.

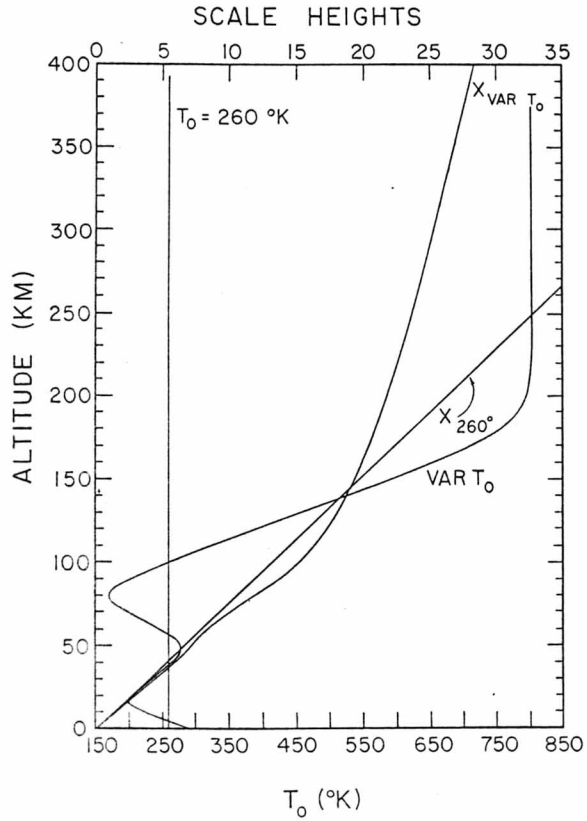

Figure 1. Various features of the basic state: T_0 for isothermal and variable temperature basic states, and height in scale heights, x, as a function of real height, z. See Sec. 2A for details.

2B. Perturbation Equations

Obtaining the linearized equations for perturbations on the basic state described above is, for the most part, a standard procedure. Only the terms $\mathscr{V}_i$, J, $\mathscr{K}$ and $\mathscr{C}$ require additional discussion. For $\mathscr{C}$, we will assume that for perturbations, δT from the basic temperature, T_0

$$\delta\mathscr{C} = a(z)\,\delta T \tag{22}$$

i.e., we adopt Newtonian cooling. This is generally an adequate approximation whenever " cooling to space " dominates radiative cooling—which, according to Rodgers and Walshaw (1966) is pretty much the rule above 4 km altitude.†

For J, we must remember that the perturbations are actually externally imposed excitations. We shall now proceed to the linearization—leaving the specification of $\mathscr{V}_i$ and $\mathscr{K}$ till later. For the moment we will only note that the perturbation expressions for $\mathscr{V}_i$ and $\mathscr{K}$ (designated by primes) will involve no coefficient dependent on horizontal coordinates or t—only on z.

Equations (1)–(6) become

$$\frac{\partial\rho'}{\partial t} + w'\frac{\mathrm{d}\rho_0}{\mathrm{d}z} + \rho_0\nabla\cdot\mathbf{v}' = 0, \tag{23}$$

$$\rho_0\frac{\partial u'}{\partial t} = -\frac{\partial p'}{\partial x_{ew}} + \mathscr{V}_{x_{ew}}' - \rho_0 D_{x_{ew}}u', \tag{24}$$

$$\rho_0\frac{\partial v'}{\partial t} = -\frac{\partial p'}{\partial y} + \mathscr{V}_y' - \rho_0 D_y v', \tag{25}$$

$$\frac{\partial p'}{\partial z} = -g\rho', \tag{26}$$

$$\rho_0 c_v\left(\frac{\partial T'}{\partial t} + w'\frac{\mathrm{d}T_0}{\mathrm{d}z}\right) = \rho_0 J' + \mathscr{K} + \frac{p_0}{\rho_0}\left(\frac{\partial\rho'}{\partial t} + w'\frac{\mathrm{d}\rho_0}{\mathrm{d}z}\right) - a(z)T', \tag{27}$$

$$\frac{p'}{\rho_0} = \frac{\rho'}{\rho_0} + \frac{T'}{T_0}, \tag{28}$$

† Cooling to space depends only on the local temperature and the amount of radiative absorber above the point in question. (22) results from linearizing the dependence on temperature.

where for Cartesian coordinates

$$\nabla \cdot \mathbf{v}' = \frac{\partial u'}{\partial x_{ew}} + \frac{\partial v'}{\partial y} + \frac{\partial w'}{\partial z}. \tag{29}$$

For correspondence with tidal theory we will seek solutions to (23)–(28) of the following form

$$\begin{Bmatrix} \rho' \\ p' \end{Bmatrix} = \mathrm{e}^{-x/2}\, \mathrm{e}^{i(\sigma t + k x_{ew})} \cos my \begin{Bmatrix} \hat{\rho}(z) \\ \hat{p}(z) \end{Bmatrix} \tag{30}$$

$$\begin{Bmatrix} u' \\ w' \\ T' \end{Bmatrix} = \mathrm{e}^{x/2}\, \mathrm{e}^{i(\sigma t + k x_{ew})} \cos my \begin{Bmatrix} \hat{u}(z) \\ \hat{w}(z) \\ \hat{T}(z) \end{Bmatrix} \tag{31}$$

and

$$v' = e^{x/2}\, e^{i(\sigma t + k x_{ew})} \sin my \quad \hat{v}(z) \tag{32}$$

For convenience, moreover, we let

$$\begin{Bmatrix} \tilde{p} \\ \tilde{\rho} \end{Bmatrix} = \frac{gH}{p_0(0)} \begin{Bmatrix} \hat{p} \\ \hat{\rho} \end{Bmatrix} \tag{33}$$

and in the equations we obtain from (23)–(28), after substituting (30)–(33), we shall drop the caps (^).† We shall also replace z by x as the vertical variable.

$$i\sigma\tilde{\rho} + \left(iku + mv + \frac{1}{H}\left(\frac{\mathrm{d}w}{\mathrm{d}x} - \left(\frac{1}{2} + \frac{1}{H}\frac{\mathrm{d}H}{\mathrm{d}x} \right) w \right) \right) = 0\,, \tag{34}$$

$$i\sigma u = -ik\tilde{p} + \frac{gH}{p_0(0)}\, \mathrm{e}^{x/2}\, \mathscr{V}'_{x_{ew}} - D_{x_{ew}} u\,, \tag{35}$$

$$i\sigma v = m\tilde{p} + \frac{gH}{p_0(0)}\, \mathrm{e}^{x/2}\, \mathscr{V}_y' - D_y v\,, \tag{36}$$

$$\frac{\mathrm{d}\tilde{p}}{\mathrm{d}x} - \left(\frac{1}{2} + \frac{1}{H}\frac{\mathrm{d}H}{\mathrm{d}x} \right) \tilde{p} = -gH\tilde{\rho}\,, \tag{37}$$

$$\begin{aligned} i\sigma T + w\left(\frac{g}{R}\frac{1}{H}\frac{\mathrm{d}H}{\mathrm{d}x} - \frac{g}{R^2}\frac{\mathrm{d}R}{\mathrm{d}x} \right) &= \frac{\gamma - 1}{R}\, \mathrm{e}^{-x/2} J' + \frac{\gamma - 1}{R}\frac{gH}{p_0(0)}\, \mathrm{e}^{x/2}\, \mathscr{K}' \\ &\quad + \frac{g(\gamma - 1)}{R}\left(i\sigma H\tilde{\rho} + \left(1 + \frac{1}{H}\frac{\mathrm{d}H}{\mathrm{d}x} \right) w \right) - aT, \end{aligned} \tag{38}$$

† In the remainder of this study we will use unprimed, uncapped symbols to represent transformed variables, and primed symbols to represent untransformed perturbations.

$$\tilde{p} = gH\tilde{\rho} + RT. \tag{39}$$

We shall solve (34)–(39) using the numerical scheme described by Lindzen and Kuo.[22] This scheme is designed for systems of coupled second order differential equations. Noting that $\mathscr{V}'_{x_{ew}}$, $\mathscr{V}_y'$ and $\mathscr{K}'$ will be second order operators on u, v and T respectively, we find that (34)–(39) are readily reduced to four coupled second order equations in u, v, T, and w. (35), (36) and (38) are already of almost the correct form. We need only express $\tilde{p}$ and $\tilde{\rho}$ in terms of u, v, T and w. (34) gives the necessary expression for $\tilde{\rho}$, and (39) with (34) yields the expression for $\tilde{p}$. Substituting these expressions into (35), (36) and (38) yields our first three final equations:

$$\begin{aligned} -\sigma^2 u = &-ik\left(-gH\left(iku + mv + \frac{1}{H}\left(\frac{\mathrm{d}w}{\mathrm{d}x} - \left(\frac{1}{2} + \frac{1}{H}\frac{\mathrm{d}H}{\mathrm{d}x} \right) w \right) \right) + i\sigma RT \right) \\ &+ \frac{i\sigma gH}{p_0(0)}\, \mathrm{e}^{x/2}\, \mathscr{V}'_{x_{ew}} - i\sigma D_{x_{ew}} u\,, \end{aligned} \tag{40}$$

$$\begin{aligned} -\sigma^2 v = &\, m\left(-gH\left(iku + mv + \frac{1}{H}\left(\frac{\mathrm{d}w}{\mathrm{d}x} - \left(\frac{1}{2} + \frac{1}{H}\frac{\mathrm{d}H}{\mathrm{d}x} \right) w \right) \right) + i\sigma RT \right) \\ &+ \frac{i\sigma gH}{p_0(0)}\, \mathrm{e}^{x/2}\, \mathscr{V}_y' - i\sigma D_y v \end{aligned} \tag{41}$$

and

$$\begin{aligned} i\sigma T = &\frac{\gamma - 1}{R}\, \mathrm{e}^{-x/2} J + \frac{\gamma - 1}{R}\frac{gH}{p_0(0)}\, \mathrm{e}^{x/2}\, \mathscr{K}' \\ &+ \frac{\gamma - 1}{R} gH\left(-\left(iku + mv + \frac{1}{H}\left(\frac{\mathrm{d}w}{\mathrm{d}x} + \left(\frac{1}{2} + \frac{1}{\gamma - 1}\frac{1}{H}\frac{\mathrm{d}H}{\mathrm{d}x} \right. \right. \right. \right. \\ &\left. \left. \left. \left. - \frac{1}{\gamma - 1}\frac{1}{R}\frac{\mathrm{d}R}{\mathrm{d}x} \right) w \right) \right) \right) - aT. \end{aligned} \tag{42}$$

The fourth equation is readily obtained from Eqs. (34), (37) and (39):

$$\begin{aligned} &\left\{ \frac{\mathrm{d}^2}{\mathrm{d}x^2} - \frac{2}{H}\frac{\mathrm{d}H}{\mathrm{d}x}\frac{\mathrm{d}}{\mathrm{d}x} - \left(\frac{1}{H}\frac{\mathrm{d}^2 H}{\mathrm{d}x^2} - \frac{2}{H^2}\left(\frac{\mathrm{d}H}{\mathrm{d}x} \right)^2 + \frac{1}{4} \right) \right\} w \\ &\quad + H\left(\frac{\mathrm{d}}{\mathrm{d}x} + \frac{1}{2} \right)(iku + mv) \\ &\quad - \frac{i\sigma R}{g}\left(\frac{\mathrm{d}}{\mathrm{d}x} - \left(\frac{1}{2} + \frac{1}{H}\frac{\mathrm{d}H}{\mathrm{d}x} - \frac{1}{R}\frac{\mathrm{d}R}{\mathrm{d}x} \right) \right) T = 0. \end{aligned} \tag{43}$$

Let $\vec{\mathscr{U}} = (u, v, T, w)$ be a vector function of x. Then (40)–(43) can be written in the form

$$\mathbf{A}\frac{\mathrm{d}^2}{\mathrm{d}x^2}\vec{\mathscr{U}} + \mathbf{B}\frac{\mathrm{d}}{\mathrm{d}x}\vec{\mathscr{U}} + \mathbf{C}\vec{\mathscr{U}} = \vec{\mathscr{D}} \tag{44}$$

where $\mathbf{A}$, $\mathbf{B}$, $\mathbf{C}$ are 4×4 matrices and $\vec{\mathscr{D}}$ is a 4-vector—all are dependent on x.

2c. $\mathscr{V}'$ AND $\mathscr{K}'$

$\mathscr{V}'$ and $\mathscr{K}'$ represent divergence of momentum and heat flux due to both molecular and eddy diffusion. The representation of eddy diffusion is an uncertain matter—given our ignorance of turbulence. We have made the simplest and most conventional choice:

$$\mathscr{V}'_{\text{eddy}} = \nu_{\text{eddy}}\,\rho_0(z)\frac{\mathrm{d}^2}{\mathrm{d}z^2}\begin{Bmatrix}u'\\v'\end{Bmatrix}, \tag{45}$$

$$\mathscr{K}'_{\text{eddy}} = K_{\text{eddy}}\,\rho_0(z)\frac{R}{\gamma-1}\frac{\mathrm{d}^2}{\mathrm{d}z^2}T', \tag{46}$$

where u', v' and T' refer to the quantities defined in Eqs. (31) and (32). ν_{eddy} and K_{eddy} can be functions of z.†

For the molecular contributions, we will, in the present study, ignore the existence of 2nd viscosities, and use the simplest elementary kinetic theory expressions appropriate to spherical molecules. From Hirschfelder, *et al.* (1954) we have

$$\mathscr{V}'_{\text{mol}} = \frac{\mathrm{d}}{\mathrm{d}z}\left(\mu\frac{\mathrm{d}}{\mathrm{d}z}\begin{Bmatrix}u'\\v'\end{Bmatrix}\right), \tag{47}$$

$$\mathscr{K}'_{\text{mol}} = \frac{\mathrm{d}}{\mathrm{d}z}\left(\kappa\frac{\mathrm{d}}{\mathrm{d}z}T'\right), \tag{48}$$

where

$$\mu = \frac{4}{15}\frac{\kappa}{R}, \tag{49}$$

† It has been properly pointed out by a reviewer that expressions (45) and (46) are physically inconsistent insofar as they are not divergences. The use of (45) and (46) amounts to neglecting a term of order $1/H$ as compared to d/dz which is approximately correct for all cases where eddy transports prove at all significant.

and

$$\kappa\alpha\frac{1}{\sigma^2}\sqrt{\frac{T}{M}}\,; \tag{50}$$

σ = collision cross-section for gas molecules.

In general σ† will vary when N does. According to Nicolet[26]

$$\kappa\sim\text{const}\,\sqrt{T}/M \tag{51}$$

in the atmosphere.

Since R is also inversely proportional to M, (51) and (49) suggest that μ is independent of M in the atmosphere. Both ν and κ are proportional to $\sqrt{T}$. In view of this, expressions (47) and (48) are not yet linearized. The linearization of (48) yields

$$\mathscr{K}'_{\text{mol}} = \kappa_0\left\{\frac{\mathrm{d}^2T'}{\mathrm{d}z^2} + \left(\frac{1}{T_0}\frac{\mathrm{d}T_0}{\mathrm{d}z} - \frac{1}{M}\frac{\mathrm{d}M}{\mathrm{d}z}\right)\frac{\mathrm{d}T'}{\mathrm{d}z} + \left(\frac{1}{2}\frac{1}{T_0}\frac{\mathrm{d}^2T_0}{\mathrm{d}z^2} - \frac{1}{4}\frac{1}{T_0^2}\left(\frac{\mathrm{d}T_0}{\mathrm{d}z}\right)^2 - \frac{1}{2}\frac{1}{M}\frac{\mathrm{d}M}{\mathrm{d}z}\frac{1}{T_0}\frac{\mathrm{d}T_0}{\mathrm{d}z}\right)T'\right)\right\}, \tag{52}$$

where $\kappa_0\,\alpha\sqrt{T_0}/M$.

Similarly

$$\mathscr{V}'_{\text{mol}} = \mu_0\left(\frac{\mathrm{d}^2}{\mathrm{d}z^2} + \frac{1}{2}\frac{1}{T_0}\frac{\mathrm{d}T_0}{\mathrm{d}z}\frac{\mathrm{d}}{\mathrm{d}z}\right)\begin{Bmatrix}u'\\v'\end{Bmatrix}. \tag{53}$$

Finally,

$$\mathscr{V}' = \mathscr{V}'_{\text{eddy}} + \mathscr{V}'_{\text{mol}}, \tag{54}$$

and

$$\mathscr{K}' = \mathscr{K}'_{\text{eddy}} + \mathscr{K}'_{\text{mol}}. \tag{55}$$

The transformation of (45), (46), (52) and (53) to x-dependence and the substitution of expressions (31) and (32) is perfectly straightforward and will not be dwelled on here. All that remains to be described is our choice of distributions for ν_{eddy} and K_{eddy}. We have chosen

$$\left.\begin{aligned}\nu_{\text{eddy}} &= 10^5\left(1+3\left(1-\frac{z}{10\text{ km}}\right)\right)\frac{\text{cm}^2}{\text{sec}} \quad \text{for} \quad z<10\text{ km}\\ &= 10^5\frac{\text{cm}^2}{\text{sec}} \quad \text{for} \quad z\geqslant 10\text{ km}\end{aligned}\right\} \tag{56}$$

† The use of σ as a collision cross-section occurs only in this section. Elsewhere σ refers to frequency.

and

$$K_{\text{eddy}} = 1.36\, \nu_{\text{eddy}} \tag{57}$$

The value of K_{eddy} near the ground was chosen to be close to values cited by Kuo.[16] The value above 10 km was chosen to be characteristic of the values commonly used for the stratosphere. However, the choice is relatively unimportant; our results for $\nu_{\text{eddy}} = 10^5$ cm^2/sec above 10 km were insignificantly different from results for $\nu_{\text{eddy}} = 10^6$ cm^2/sec or even $\nu_{\text{eddy}} = 0.0$ above 10 km.

We took κ mol $= 9.3 \times 10^{-3}$ gm km/deg sec at the ground. A more accurate choice would not significantly alter our results.

The insensitivity to our choice of K_{eddy} will be briefly demonstrated in Section 3 and in greater detail in Part II. Horizontal diffusion proved negligibly small, and was neglected.

2D. Radiative Cooling

Radiative cooling, as represented by Newtonian cooling in our model, is due to infrared emission by water vapor in the troposphere and by carbon dioxide above the tropopause (with a smaller contribution from ozone in the stratosphere).[25,28] There is also a small contribution from atomic oxygen in the lower thermosphere.[3] The temperature dependence of radiative cooling above about 70 km diminishes markedly due to the breakdown of local thermodynamic equilibrium for CO_2.[25] Lindzen and Goody[21] suggested that ozone photochemistry (which for oxygen allotrope reactions is very temperature dependent) could lead to a great increase in Newtonian cooling near 40 km. However, recent studies[14] suggest that hydrogen–oxygen reactions (which are not temperature dependent) are dominant. In general, there is considerable uncertainty as to the best choice for $a(z)$. However, as we shall show in Part II, the effect of Newtonian cooling is not profound, and, hence, the choice of $a(z)$ is not critical. We have chosen

$$a(z) = \left\{0.586 \times 10^{-6} \exp\left(-\left(\frac{z}{100\text{ km}}\right)^2\right) + 2.9 \times 10^{-6} \exp\left(-\left(\frac{z - 80\text{ km}}{50\text{ km}}\right)^2\right)\right\} \tag{58}$$

The units of $a(z)$ are 1/time. Newtonian cooling is locally important when $a(z) \gtrsim \sigma$; it is also important for wave transmission over paths whose length L is greater than $\sigma 1/a$ where 1 is a characteristic wavelength.[20] Only the latter possibility is of importance in the present study.

2E. Ion Drag

Within the F-region of the ionosphere ions are relatively numerous —and more important, their gyromagnetic frequency is large compared to their collision frequency with neutral molecules. Thus the ions are constrained to move mainly along magnetic field lines, and neutral molecules moving across field lines must, in effect, move through a stationary mesh of ions, which must, in turn, exert a drag on the neutral molecules. The simplest expression for the drag (and the most commonly used expression[6,15,17] is that used in Eqs. (2) and (3) where

$$D_{x_{ew}} = \text{const} \times \sin \phi_{x_{ew}} \times N_i \tag{59}$$

$$D_y = \text{const} \times \sin \phi_y \times N_i \tag{60}$$

and where const $= 5 \times 10^{-9}$ cm^3/sec,

N_i = number density of ions,

$\phi_{x_{ew}}$ = angle between x-axis and magnetic field line,

ϕ_y = angle between y-axis and magnetic field line.

In general N_i is a function of time, varying greatly in the course of a day. In the present study, however, we shall take N_i to be stationary in time corresponding to an average over the whole day. Our distribution of N_i will be of the following form

$$N_i = N_{i\max} \exp\left[-\left(\frac{z - z_c}{L}\right)^4\right] \tag{61}$$

where $N_{i\max} = 10^6$ cm^{-3}

$L = 150$ km,

z_c = height at which $N_i = N_{i\max}$.

Our choice for $N_{i\max}$ corresponds to a very high average ion density and the thickness we have chosen for the heavily ionized region is greater than is normally encountered. z_c is left open. As for $\phi_{x_{ew}}$ and ϕ_y, we shall in this study take

$$\phi_{x_{ew}} = \frac{\pi}{2} \quad \text{and} \quad \phi_y = 0.\dagger$$

As with $a(z)$, the dimensions of $D_{x_{ew}}$ and D_y are 1/Time. However, this time $D_{x_{ew}} \gg \sigma$. Nevertheless, the anisotropy of the ion drag makes the simple use of this dimensional consideration misleading. We shall show this later; we shall find that when molecular viscosity is included, z_c is the most important parameter in determining the importance of ion drag. For most reasonable choices of z_c, it turns out that the effects of ion drag are relatively small—primarily because viscosity dominates both inertia and ion drag within the F-region. Thus, the precise specification of ion drag may not prove to be very important. This conclusion must remain tentative since simple drag is only one manifestation of hydromagnetic effects, and a full consideration of the problem has not yet been attempted.

2F. Thermal Excitation

In Part I, we consider waves arbitrarily excited below 90 km. Hence, we will defer our discussion of J to Parts II and III.

2G. Lower Boundary Conditions

We are taking our lower boundary to be a flat, rigid, perfectly conducting surface upon which we may specify a temperature oscillation δT_{gnd} with frequency σ. For an adiabatic, inviscid fluid the natural boundary condition is

$$w = 0 \quad \text{at} \quad z = 0. \tag{62}$$

When viscosity, conductivity (and anisotropy in ion drag) are allowed, we need 3 additional lower boundary conditions. It might be supposed that no slip (i.e. $u(0) = v(0) = 0$) and $T(0) = \delta T_{gnd}$ would be appropriate—but this is not the case.

The values of eddy conductivity and viscosity we have at the ground are really applicable above some height of order 10 m. From the ground to this height the effective viscosity and conductivity

† This choice would be appropriate to the equator if the geomagnetic equator coincided with the geographical equator. While our choice is not realistic in the details of the anisotropy, it is hoped that by adopting a larger than average value for the magnitude of the ion drag we can meaningfully determine how important ion drag might be.

rise from their molecular values to values like those we have adopted at $z = 0$. Rather than attempt to resolve adequately the atmosphere's lower 10 m, we adopt slip boundary conditions for velocity and temperature at $z = 0$. The simplest form for these is:

$$\frac{\mathrm{d}}{\mathrm{d}z}\begin{pmatrix} u' \\ v' \\ T' \end{pmatrix} = c_s \times \begin{pmatrix} u' \\ v' \\ T' \end{pmatrix} \quad \text{at} \quad z = 0. \tag{63}$$

We use (63) for most of our calculations. We chose c_s in order to simulate some of Kuo's[16] results for the transmission of surface temperature oscillations to the atmospheric boundary layer:

$$c_s = 1.7 \text{ cm sec}^{-1}/\nu_{\text{eddy}}(0)$$

In the course of our calculations we found that the choice of lower boundary conditions for u', v' and T' has little effect on our results for thermal excitation above the ground. This will be simply demonstrated in Section 3. In Part II we will discuss the physical basis for a lower boundary condition and the effect of the lower boundary conditions on the atmospheric oscillations induced by surface temperature oscillations. For the results discussed in Part I the lower boundary conditions are of no importance.

2H. Upper Boundary Conditions

For inviscid, adiabatic fluids the upper boundary condition is either the requirement that solutions be bounded—or if this does not uniquely determine a solution then a radiation condition is imposed (i.e., it is assumed that no energy is coming down from infinity). Behind the latter choice is the assumption that the increasing importance of molecular viscosity and conductivity in the upper atmosphere will serve to absorb upward travelling waves. As we shall see, this is approximately the case in most realistic cases; however, as Yanowitch[36] has shown, there are conditions under which increasing viscosity as an inhomogeneity in the medium can cause significant wave reflection. A discussion of the radiation condition and its numerical treatment may be found in Lindzen and Chapman.[20]

In the present study we find that as z (or x) approach infinity,

equations (40), (41) and (42) asymptotically become

$$\mathscr{V}'_{x_{ew}} = 0 \tag{64}$$

$$\mathscr{V}'_{y} = 0 \tag{65}$$

and

$$\mathscr{K}' = 0. \tag{66}$$

Using (45) (46), (52) and (53) and recognizing that both dT_0/dz and dM/dz approach zero as $z \to \infty$ in our model, (64)–(66) become

$$\frac{d^2u'}{dz^2} = 0 \tag{67}$$

$$\frac{d^2v'}{dz^2} = 0 \tag{68}$$

and

$$\frac{d^2T'}{dz^2} = 0 \tag{69}$$

The solutions to (67)–(69) are all of the form $az + b$, where a and b are constants. If there is to be no flux of horizontal momentum or heat from infinity, then the solutions must, in fact, approach a simple constant. In our numerical treatment we require that

$$\frac{du'}{dz} = \frac{dv'}{dz} = \frac{dT'}{dz} = 0 \tag{70}$$

at some finite height. This procedure is adequate provided that the resulting solutions approach a constant well below the top level. For a top at $x = 35$, this was, indeed, the case for all waves studied. In terms of our transformed variables (70) becomes

$$\left(\frac{d}{dx} + \frac{1}{2}\right)\begin{pmatrix} u \\ v \\ T \end{pmatrix} = 0 \tag{71}$$

$$\text{at} \quad x = 35.$$

Equation (71) provides only three upper boundary conditions; a fourth is needed. This is obtained from (43) with (71), and taking $dH/dx = dR/dx = 0$:

$$\left(\frac{d}{dx} + \frac{1}{2}\right) w = \frac{i\sigma R}{g} T \tag{72}$$

$$\text{at} \quad x = 35.$$

It is easily shown that (72) implies that w' (the physical, untransformed variable) increases linearly with height at great heights instead of approaching a constant. This may seem surprising, but it is merely an expression of the fact that in an exponentially stratified, hydrostatic atmosphere whose temperature and composition do not vary with height above some level but whose temperature oscillates with time, the vertical displacement of material surfaces increases linearly with height. It can be shown that the same must be true for oscillations in pressure and density at a given point, and this is confirmed by analysis of the data in Harris and Priester (1965) for the quantity, $(1/\rho_0)(\partial p/\partial x_{ew})$.[17]

21. Tidal Modes and "Equivalent" Gravity Waves

If we set $\mathscr{V}'_{x_{ew}} = \mathscr{V}'_{y} = D_x = D_y = \mathscr{K}' = a = 0$, then Eqs. (23), (26), (27) and (28) are exactly the equations used in classical tidal theory.[20] Equations (24), (25) and the expression for the divergence of the velocity must be replaced by expressions appropriate to a spherical rotating atmosphere:

$$\frac{\partial u'}{\partial t} - 2\omega v' \sin\theta = -\frac{1}{r\cos\theta}\frac{\partial}{\partial\phi}\left(\frac{p'}{\rho_0}\right), \tag{73}$$

$$\frac{\partial v'}{\partial t} + 2\omega u' \sin\theta = -\frac{1}{r}\frac{\partial}{\partial\theta}\left(\frac{p'}{\rho_0}\right), \tag{74}$$

and

$$\nabla\cdot\mathbf{v}' = \frac{1}{r\cos\theta}\frac{\partial}{\partial\theta}(v'\cos\theta) + \frac{1}{r\cos\theta}\frac{\partial u'}{\partial\phi} + \frac{\partial w'}{\partial z}, \tag{75}$$

where u' = westerly velocity
v' = southerly velocity
ω = the rotation rate of the earth
ϕ = longitude
θ = latitude
r = radius of the solid earth.

t and ϕ dependence of the form $e^{i(\sigma t + s\phi)}$ is assumed; $s = 0, \pm 1, \pm 2, \ldots$. Equations (73) and (74) are used to solve for u' and v' in terms of p'. The velocity divergence can then be rewritten

$$\nabla \cdot \mathbf{v}' = \frac{i\sigma}{4r^2\omega^2} F\left[\frac{p'}{\rho_0}\right] + \frac{\partial w'}{\partial z}, \tag{76}$$

where F is a complicated operator in θ with parametric dependence on σ and s. Equation (76) is used to eliminate u' and v' from the remaining equations. θ dependence is separated out by means of Laplace's Tidal Equation

$$F\left[\frac{p'}{p_0}\right] = -\frac{4r^2\omega^2}{gh_n^{\sigma,s}} \frac{p'}{p_0}, \tag{77}$$

When we require that p' be bounded at the poles, (77) forms an eigenfunction–eigenvalue problem whose eigenvalues for a given choice of σ and s are $\{h_n^{\sigma,s}\}_{all\ n}$, the set of equivalent depths. Each n corresponds to a different latitude mode. For σ's and s's relevant to atmospheric tides extensive tabulations of the solutions to (77) have been made—most notably by Flattery[5]—some of which are reproduced by Lindzen and Chapman.[20]

In order to find the internal gravity wave " equivalent " to a tidal mode of frequency σ, zonal wavenumbers s, and equivalent depth h, we take the same value of σ; for k we choose the zonal wavenumber of the tidal mode at the equator—namely

$$k = \frac{s}{r} \tag{78}$$

We then use Eqs. (24) and (25) where $\mathscr{Y}' = D = 0$ to express the horizontal divergence in terms of p'/ρ_0. This yields

$$\frac{\partial u'}{\partial x_{ew}} + \frac{\partial v'}{\partial y} = -\frac{i}{\sigma}(k^2+m^2)\frac{p'}{\rho_0} \tag{79}$$

A comparison of (79) with (77) permits us to determine the equivalent depth of an internal gravity wave in a plane rotating atmosphere:

$$h = \frac{\sigma^2/g}{(k^2+m^2)} \tag{80}$$

Our final step is to choose m so that the equivalent depth for the gravity wave is equal to that of the tidal mode we wish to simulate. For the diurnal tide there are important modes with negative equivalent depths. These are simulated by taking m to be imaginary. In such cases $\cos my$ in Eqs. (30) and (31) is replaced by $\cosh |m| y$ and $\sin my$ in (32) is replaced by $\sinh |m| y$.

The reader will notice from Eq. (80) that a given h may result from an infinite number of different choices for σ, k and m. We have chosen σ to be equal to that of the tidal mode because when dissipative processes are included, the frequency determines the height at which various processes become important—if they become important at all. We choose k according to (78) in order that the " equivalent " gravity waves will be approximations to the tidal modes at the equator. Therefore, m, is our only adjustable parameter.

In Table 1 we list the equivalent depths for the tidal modes we will simulate, together with the values of σ, k and m for the " equivalent " gravity waves. Also shown are the values of σ and k for the 3-hour oscillation—$m = 0$ for this case. A more detailed discussion of the correspondence between tidal modes and " equivalent " gravity waves will be given in Part II.

TABLE 1 Parameters for Tidal Modes (frequency σ, zonal wavenumber, s, and equivalent depth, h) and " Equivalent " Gravity Wave (zonal and meridional wavenumbers, k and m). Also shown is the vertical wavelength, L, of each mode in an isothermal, inviscid, adiabatic atmosphere.

Mode	σ	s	h (km)	k(km^{-1})	m (km^{-1})	L[1] (km)
1st symmetric semidiurnal	π/6 hr	2	7.85	3.14×10^{-4}	4.2×10^{-4}	293.0
2nd symmetric semidiurnal	π/6 hr	2	2.11	3.14×10^{-4}	0.96×10^{-3}	53.4
1st symmetric propagating diurnal	π/12 hr	1	0.699	1.57×10^{-4}	8.64×10^{-4}	28.3
1st symmetric trapped diurnal	π/12 hr	1	−12.25	1.57×10^{-4}	2.62×10^{-4}	---[2]
3-hour wave	π/1.5 hr		0.64	7.35×10^{-3}	0.0	26.8

[1] Vertical wavelength for isothermal T_0 (and no dissipation); needed for Sec. 5.

[2] This mode is evanescent in the vertical.

The above essentially completes the discussion of our model. We now turn to a brief description of our numerical method of solution.

3. Numerical Method of Solution

Our numerical method is designed specifically for equations of the form of Eq. (44).†

The first step is to divide our x domain into discrete intervals of length δx, labelling the gridpoints between intervals by integers n: i.e., $n = \hat{n}$ corresponds to $x = \hat{n}\,\delta x$. The subscript n will denote a function evaluated at gridpoint n. Next we replace derivatives by their finite difference approximations:

$$\left(\frac{\mathrm{d}}{\mathrm{d}x}\vec{\mathscr{U}}\right)_n \doteq \frac{\vec{\mathscr{U}}_{n+1} - \vec{\mathscr{U}}_{n-1}}{2\delta x}, \tag{84}$$

and

$$\left(\frac{\mathrm{d}^2}{\mathrm{d}x^2}\vec{\mathscr{U}}\right)_n = \frac{\vec{\mathscr{U}}_{n+1} - 2\vec{\mathscr{U}}_n + \vec{\mathscr{U}}_{n-1}}{(\delta x)^2}. \tag{85}$$

Substitution of (84) and (85) into (44) gives us a set of difference equations:

$$\tilde{\mathbf{A}}_n\vec{\mathscr{U}}_{n+1} + \tilde{\mathbf{B}}_n\vec{\mathscr{U}}_n + \tilde{\mathbf{C}}_n\vec{\mathscr{U}}_{n-1} = \vec{D}_n, \tag{86}$$
$$n = 0, 1, 2, \ldots N$$

† In practice, we did not use x as our dependent variable. Instead we used

$$y = a\left(1 - \frac{b}{x+b}\right) + x, \tag{81}$$

which, for suitable choices of a and b allows extra resolution near the surface while taking uniform grid intervals in y. This permits adequate resolution in the surface boundary layer. Our particular choice was $a = 7$, and $b = 0.25$. Thus a top at $x = 35$ corresponds to $y \cong 42$. If we take n grid intervals per unit y variation, then we will have $3.75n$ intervals in the first quarter of a scale height. When using (80)

$$\frac{\mathrm{d}}{\mathrm{d}x} = F1\frac{\mathrm{d}f}{\mathrm{d}y} \tag{82}$$

$$\frac{\mathrm{d}^2}{\mathrm{d}x^2} = -F2\frac{\mathrm{d}f}{\mathrm{d}y} + F1^2\frac{\mathrm{d}^2f}{\mathrm{d}y^2} \tag{83}$$

where $$F1 = 1 + \frac{ab}{(x+b)^2}$$

and $$F2 = \frac{2ab}{(x+b)^3}.$$

Substitution of (82) and (83) into (44) leaves us with an equation of exactly the same form as (44).

where $\tilde{\mathbf{A}}_n = \mathbf{A}_n + \frac{\delta x}{2}\mathbf{B}_n$

$\tilde{\mathbf{B}}_n = -2\mathbf{A}_n + \mathbf{C}_n(\delta x)^2$

$\tilde{\mathbf{C}}_n = \mathbf{A}_n - \frac{\delta x}{2}\mathbf{B}_n$

$\vec{D}_n = \vec{\mathscr{D}}_n(\delta x)^2$

and N = index of top grid point.

Assuming δx is sufficiently small for (84) and (85) to be adequate approximations, then our problem is reduced to the solution of $N+1$ linear algebraic vector equations (i.e., (86)) in the $N+1$ unknown vectors $\vec{\mathscr{U}}_n$, $n = 0, 1, 2, \ldots N$. The procedure for doing this is given in Lindzen and Kuo.[22] Briefly, we introduce a set of new matrices $\boldsymbol{\alpha}_n (n = 0, \ldots, N)$ and vectors $\vec{\beta}_n$ $(n = 0, \ldots, N)$ defined by the following equation

$$\vec{\mathscr{U}}_n = \boldsymbol{\alpha}_n\vec{\mathscr{U}}_{n+1} + \vec{\beta}_n. \tag{87}$$

Also,

$$\vec{\mathscr{U}}_{n-1} = \boldsymbol{\alpha}_{n-1}\vec{\mathscr{U}}_n + \vec{\beta}_{n-1}. \tag{88}$$

Substitution of (88) into (86) and comparison with (87) gives us

$$\boldsymbol{\alpha}_n = -(\tilde{\mathbf{A}}_n\boldsymbol{\alpha}_{n-1} + \tilde{\mathbf{B}}_n)^{-1}\tilde{\mathbf{C}}_n, \tag{89}$$

$$\vec{\beta}_n = (\tilde{\mathbf{A}}_n\boldsymbol{\alpha}_{n-1} + \tilde{\mathbf{B}}_n)^{-1}(\vec{D}_n - \tilde{\mathbf{A}}_n\vec{\beta}_{n-1}). \tag{90}$$

Thus, if we know $\boldsymbol{\alpha}_0$ and $\vec{\beta}_0$ we may find all the remaining $\boldsymbol{\alpha}_n$'s and $\vec{\beta}_n$'s by repeatedly inverting 4×4 matrices (a particularly simple task —especially since the matrices prove to be well conditioned). $\boldsymbol{\alpha}_0$ and $\vec{\beta}_0$ are directly determined by comparing our lower boundary conditions (62) and (63) with (87) after replacing first derivatives as follows

$$\frac{\mathrm{d}f}{\mathrm{d}x} = H\frac{\mathrm{d}f}{\mathrm{d}z} = \frac{f_1 - f_0}{\delta x}. \tag{91}$$

Having found $\boldsymbol{\alpha}_n$ and $\vec{\beta}_n$ $(n = 0, 1, 2, \ldots, N-1)$, we may find all the $\vec{\mathscr{U}}_n$'s from (88)—provided we know $\vec{\mathscr{U}}_N \cdot \vec{\mathscr{U}}_N$ is determined from our upper boundary conditions. Equations (71) and (72) may be written, more generally, in the form

$$\frac{\mathrm{d}}{\mathrm{d}x}\vec{\mathscr{U}} = \mathscr{M}\vec{\mathscr{U}}, \tag{92}$$

or in finite difference form

$$(I - \mathcal{M}_N \delta x)\vec{\mathcal{U}}_N = \vec{\mathcal{U}}_{N-1}. \tag{93}$$

Substituting (93) into (90) we get

$$(I - \vec{\mathcal{M}}_N \delta x - \alpha_{N-1})\vec{\mathcal{U}}_N = \vec{\beta}_{N-1}$$

or

$$\vec{\mathcal{U}}_N = (I - \mathcal{M}_N \delta x - \alpha_{N-1})^{-1}\vec{\beta}_{N-1} \tag{94}$$

Thus, our problem is solved.

Our numerical procedure has been specifically designed for problems where viscosity and conductivity are non-zero. When viscosity and conductivity are set equal to zero some slight modifications are necessary in the boundary conditions. For our lower boundary conditions (62) remains valid, but (63) must be replaced. Equations (40)–(42) (with $\mathscr{V}_{x'_{ew}} = \mathscr{V}_{y'} = \mathscr{K}' = 0$) are solved for u, v and T' in terms of w and dw/dx, and these relations are used instead of lower boundary conditions. Our upper boundary conditions are replaced by radiation or boundedness conditions (according to whether we are dealing with propagating or trapped modes) applied individually to u, T' and w. These conditions are also of the form of (92) (see Lindzen and Chapman[20]). Not surprisingly, inviscid, non-conducting calculations required smaller mesh sizes than viscous calculations. Also, modes associated with small values of h (equivalent depth) required smaller mesh sizes than modes with larger values of h (i.e., the shorter the inviscid vertical wavelength, the greater the resolution needed). Thus, of the five modes we are studying, the propagating diurnal and the 3-hour modes require the smallest mesh sizes. In Fig. 2 we show some of the effects of resolution on calculations for the diurnal propagating mode excited by water vapor insolation absorption (for the moment we need only note $J\alpha\, e^{-x/3}$) in an inviscid, adiabatic atmosphere with a variable basic temperature as shown in Fig. 1. Shown are solutions for $\delta y = 0.0042$, 0.01 and 0.0167. All the solutions grew approximately as $e^{x/2}$ and displayed approximately the correct phase variation with height. However, we needed $\delta y < 0.008$ in order to eliminate spurious numerical wiggles.†

† Further increases in resolution beyond $\delta y \sim 0.008$ produced only slight changes in the results. It appears to be characteristic of this method that the transition from totally inadequate to adequate resolution occurs suddenly.

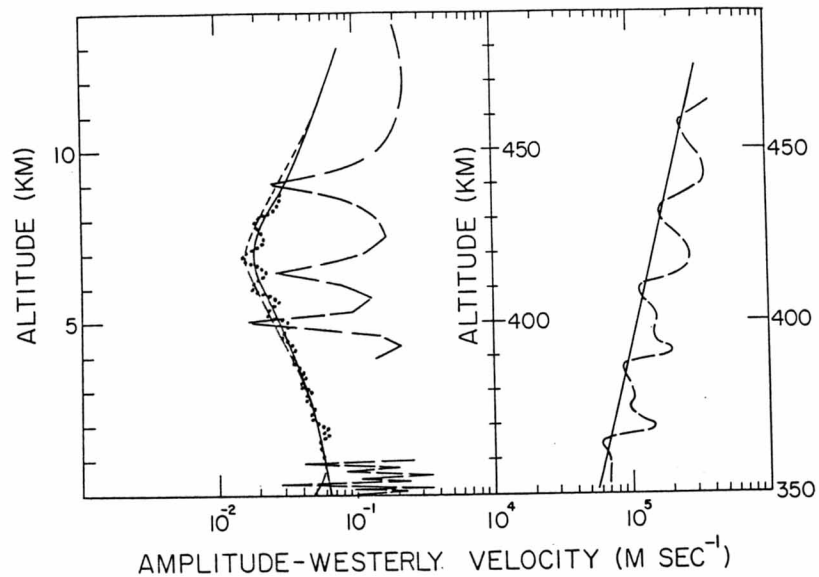

Figure 2. Amplitude of u' as a function of height (for the regions 0–15 km and 350–450 km) for the diurnal propagating mode. Shown are results for model (iii) obtained using various resolutions: $\delta y = 0.0167$ ——, $\delta y = 0.01$ ·····, $\delta y = 0.0042$ ———. Also shown are results for an " almost " inviscid atmosphere with $\delta y = 0.0042$ – – – – – –. See Sec. 3 for details.

For $\delta y > 0.02$ the numerical solutions actually decreased with height—the numerical solutions becoming nonsense. Also shown in Fig. 2 are the results of calculations for an atmosphere with no molecular viscosity and conductivity, but with eddy viscosity given by

$$\nu_{\text{eddy}} = \left(10^3 + 3.99 \times 10^5\left(1 - \frac{z}{10}\,\text{km}\right)\right) \text{cm}^2/\text{sec} \quad \text{for} \quad z < 10 \text{ km}$$

$$= 10^3 \text{ cm}^2/\text{sec} \quad \text{for} \quad z \geqslant 10 \text{ km} \tag{95}$$

instead of (56). K_{eddy} is given by (57). (95) represents normal eddy diffusion in the lower troposphere but negligible eddy diffusion above 10 km. (In the figure legend we refer to this case as " almost inviscid ".) We see that the " almost inviscid " and the inviscid solutions are identical above 10 km. Between 1 km and 10 km the amplitude of the solution in an " almost inviscid " atmosphere is slightly less than in an inviscid atmosphere. Only in the lowest kilometer of the atmosphere is there a somewhat significant difference

in the solutions. These results show that the lower boundary condition cannot be overwhelmingly important for oscillations excited within the atmosphere.† They also show that slight viscosity has negligible effect. Significantly the presence of slight viscosity reduces the resolution needed for an accurate solution.

4. Overall Results

We have calculated vertical distributions of the amplitude and phase of u', v', w', T', $\delta p'/\rho_0$ and $\delta p'/p_0$ for the five gravity waves described in Table 1. For each mode we have investigated the following models.

(i) An isothermal atmosphere where $T_0 = 260\,^\circ\text{K}$. $M = 28.9 =$ constant, and viscosity, conductivity and ion drag are omitted.

(ii) An isothermal atmosphere where $T_0 = 260\,^\circ\text{K}$. $M = 28.9 =$ constant; viscosity and conductivity as described in Section 2c are included. However, ion drag is omitted.

(iii) An atmosphere with variable T_0 as shown in Fig. 1 and variable M and γ as given by Eqs. (20) and (21). Viscosity, conductivity and ion drag are omitted.

(iv) Same as (iii) but ion drag is included with ion drag with $z_c = 350$ km (see Eq. (61)).

(v) Same as (iii) but with viscosity and conductivity as described in Section 2c and no ion drag.

(vi) Same as (v) but with ion drag with $z_c = 350$ km.

(vii) Same as (v) but with ion drag with $z_c = 320$ km.

Figure 3 shows the distribution of the amplitude of u' with height for each of the seven models described above for a gravity wave corresponding to the first symmetric propagating diurnal tidal mode. Figure 4 shows the distributions of the phase of u' for the same mode and each of the models. Figures 5 and 6 show the distributions of the amplitudes of v' and T' respectively for the diurnal propagating (positive equivalent depth) mode. Figures (7)–(10) show the same quantities for the trapped (negative h) diurnal mode; Figs. (11)–(14) for the first semidiurnal mode; Figs. (15)–(18) for the second semidiurnal mode; and Figs. (19)–(21) for the 3-hr wave. $v' = 0$ for the

† This conclusion is inferred from the fact that outside of the boundary layer it does not matter whether we have a viscous boundary layer or not

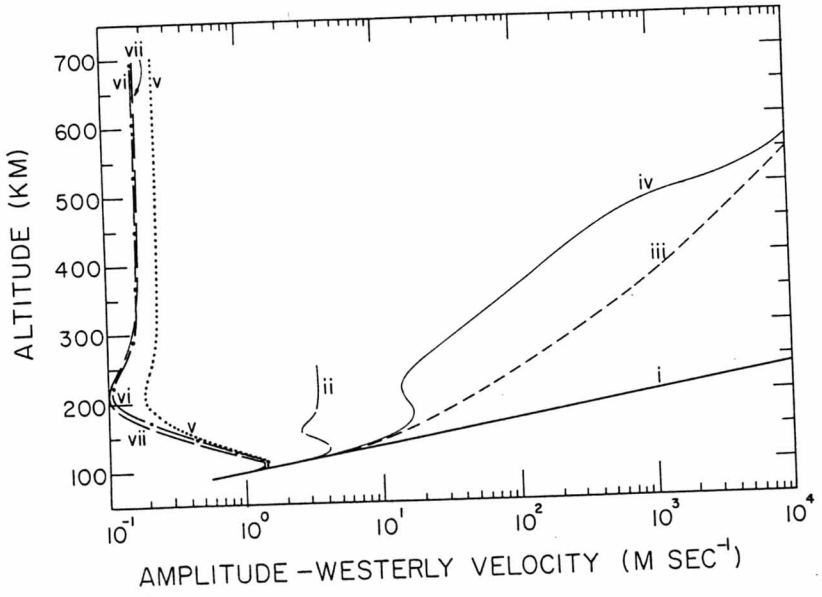

Figure 3. Amplitude of u' for the propagating diurnal mode as a function of height using models (i)–(vii).

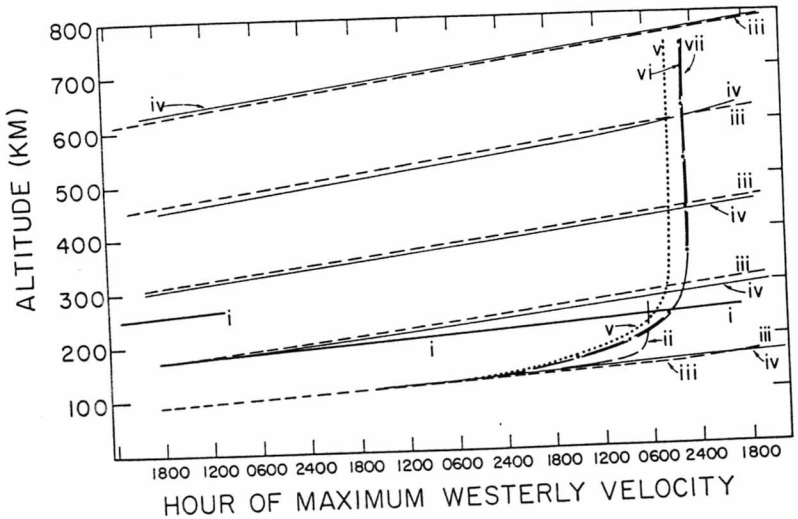

Figure 4. Phase of u' for the propagating diurnal mode as a function of height using models (i)–(vii).

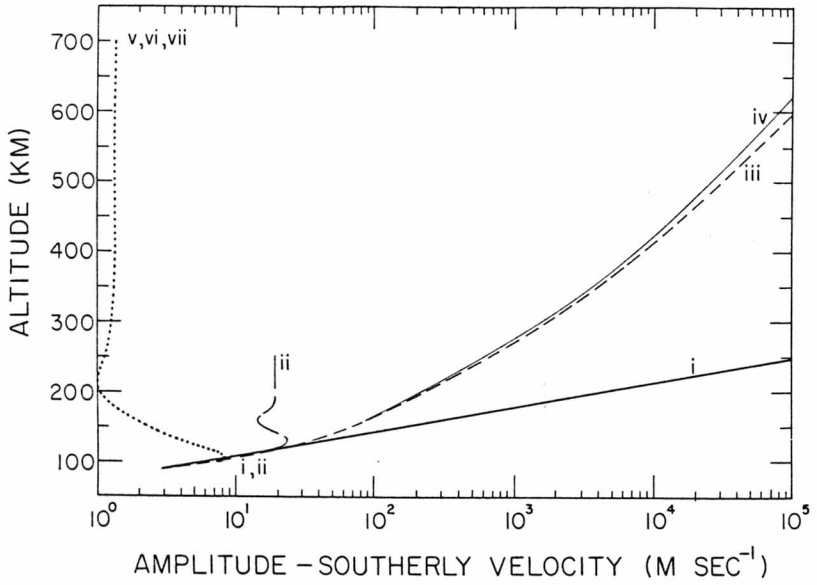

Figure 5. Amplitude of v' for the propagating diurnal mode as a function of height using models (i)–(vii).

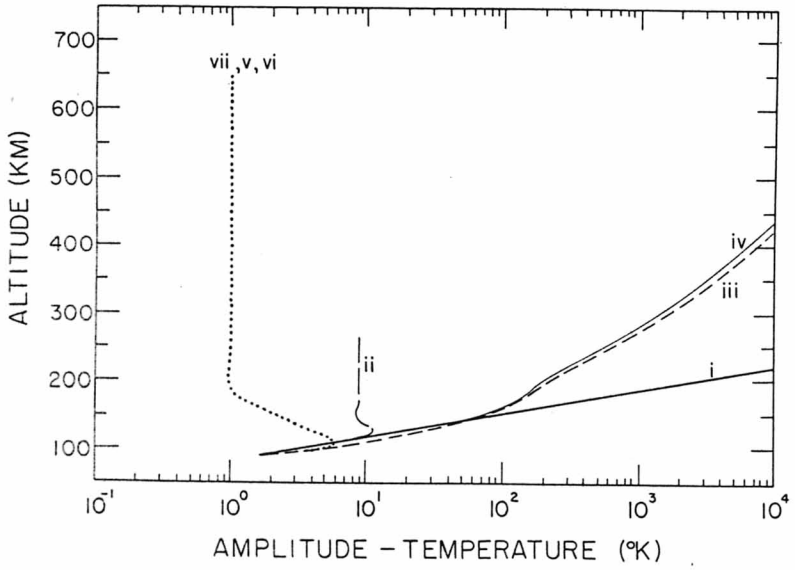

Figure 6. Amplitude of T' for the propagating diurnal mode as a function of height using models (i)–(vii).

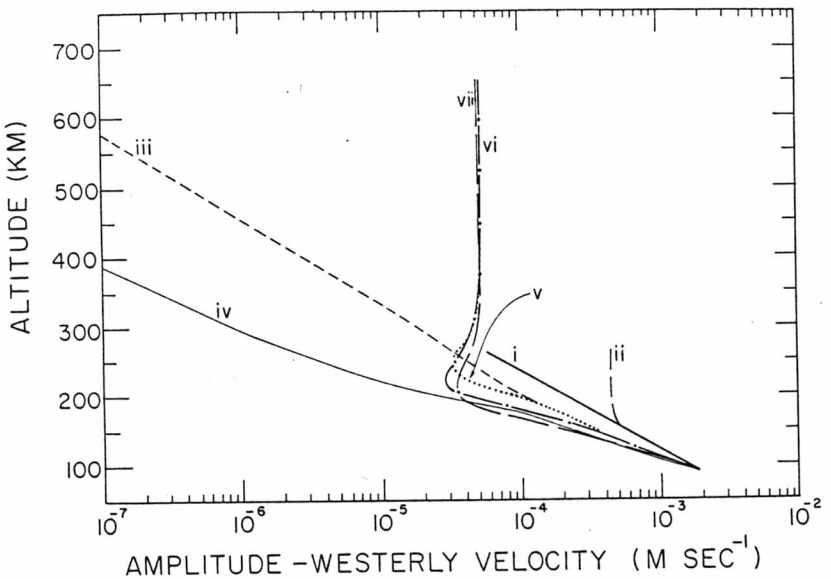

Figure 7. Same as Fig. 3—but for the trapped diurnal mode.

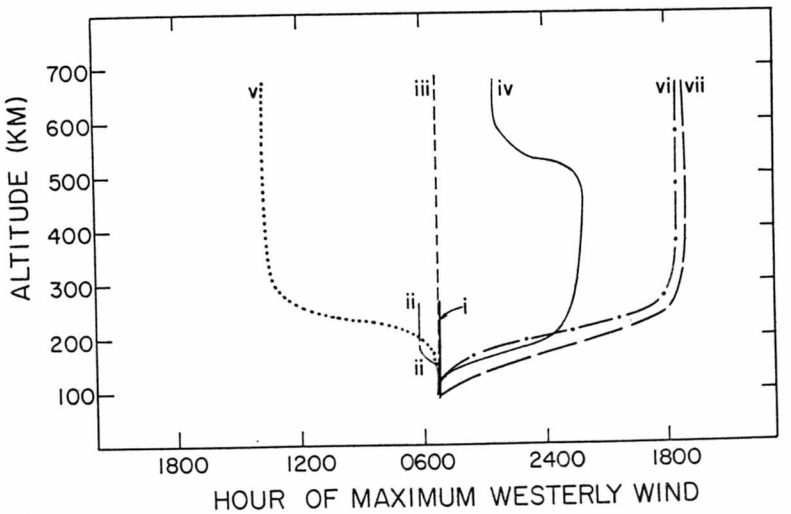

Figure 8. Same as Fig. 4—but for the trapped diurnal mode.

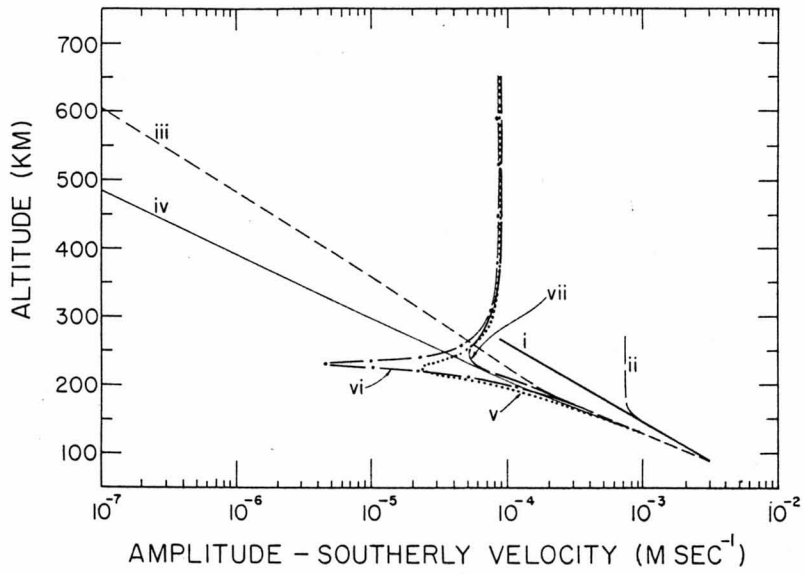

Figure 9. Same as Fig. 5—but for the trapped diurnal mode.

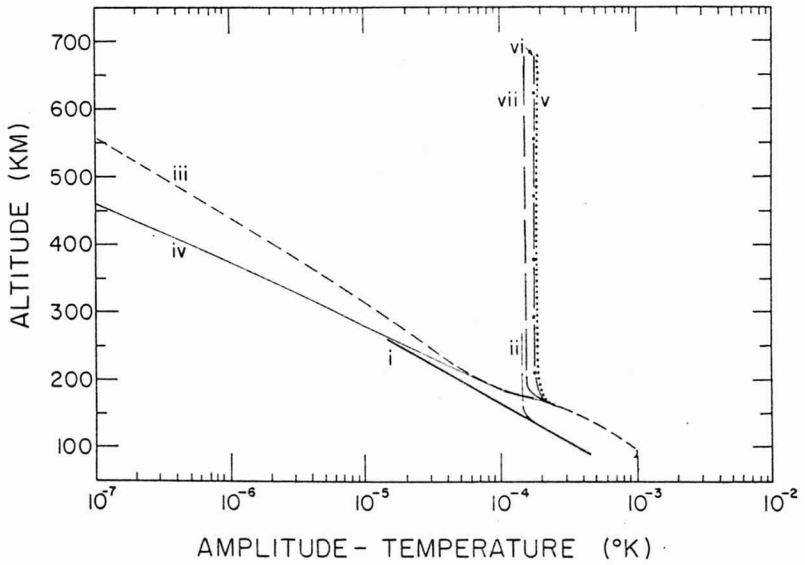

Figure 10. Same as Fig. 6—but for the trapped diurnal mode.

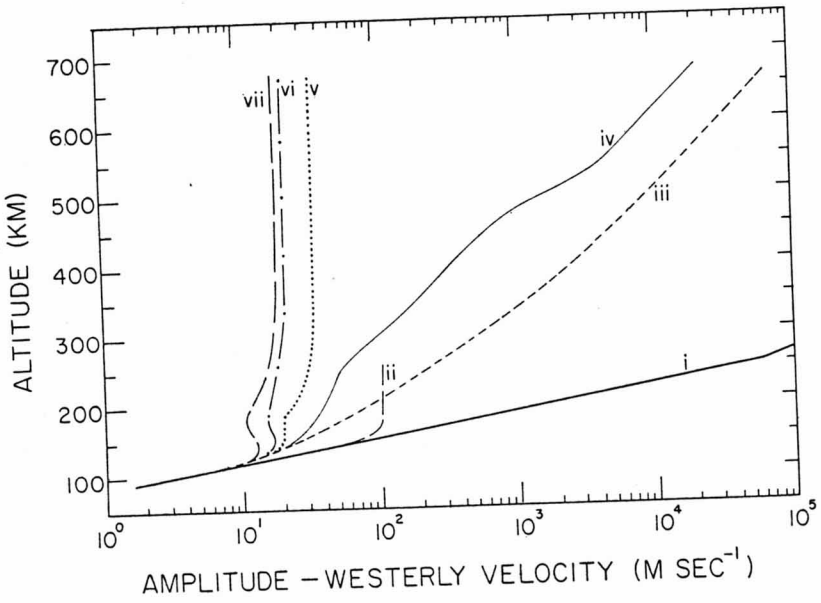

Figure 11. Same as Fig. 3—but for the first semidiurnal mode.

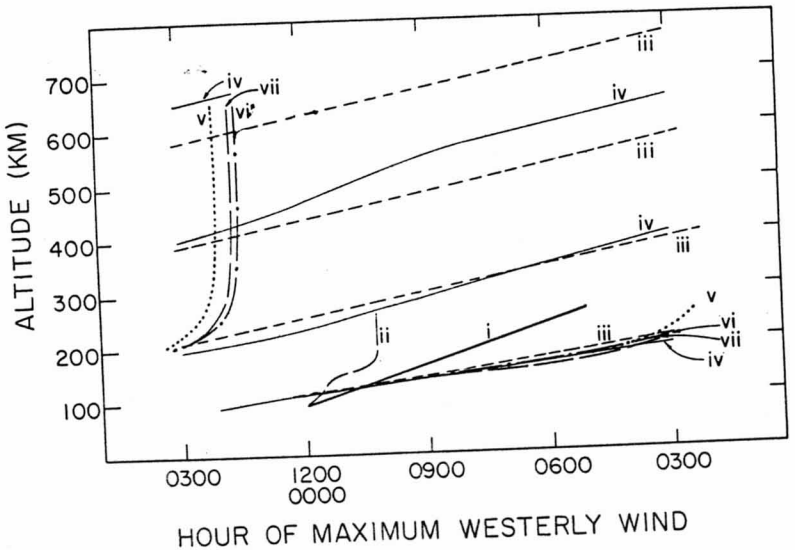

Figure 12. Same as Fig. 4—but for the first semidiurnal mode.

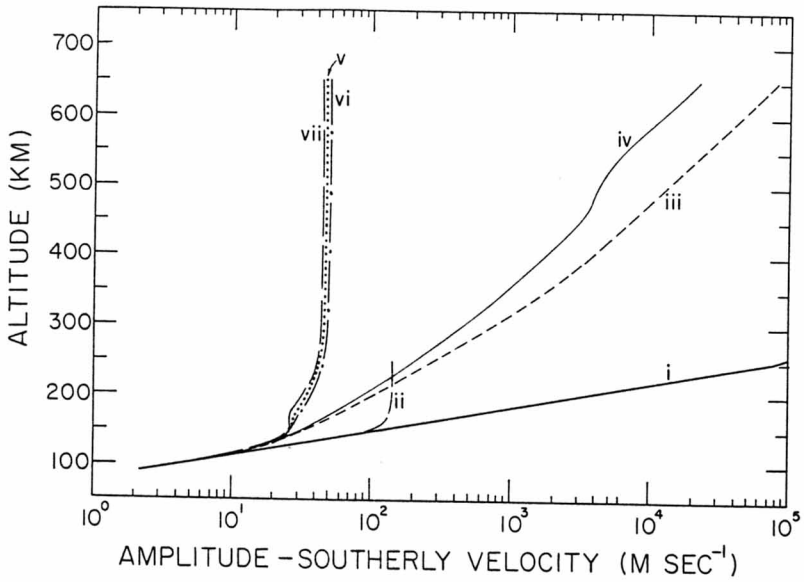

Figure 13. Same as Fig. 5—but for the first semidiurnal mode.

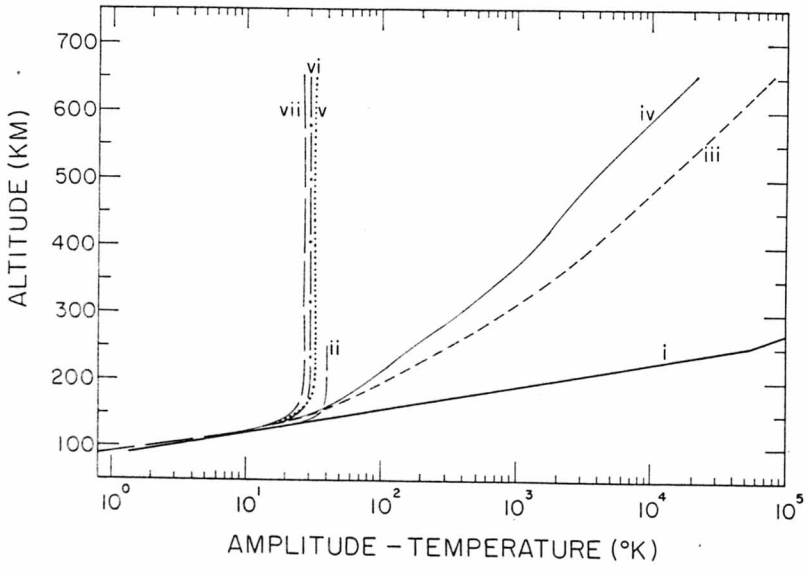

Figure 14. Same as Fig. 6—but for the first semidiurnal mode.

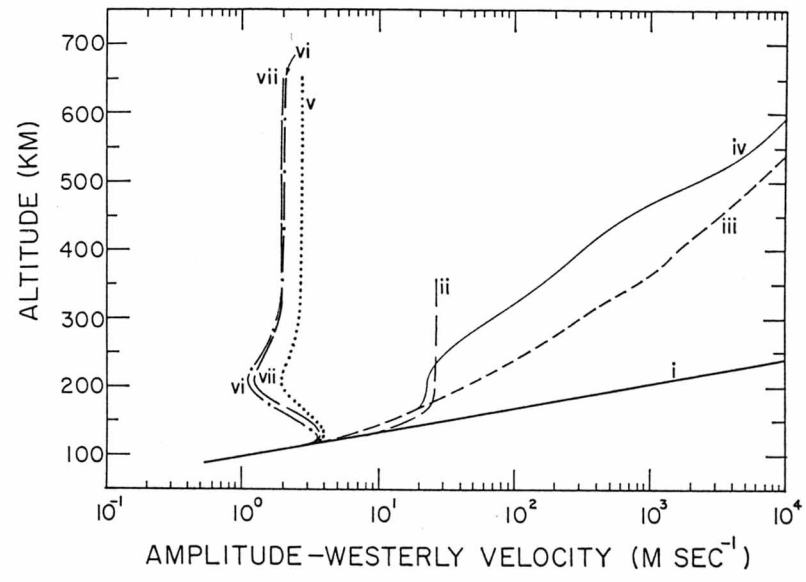

Figure 15. Same as Fig. 3—but for the second semidiurnal mode.

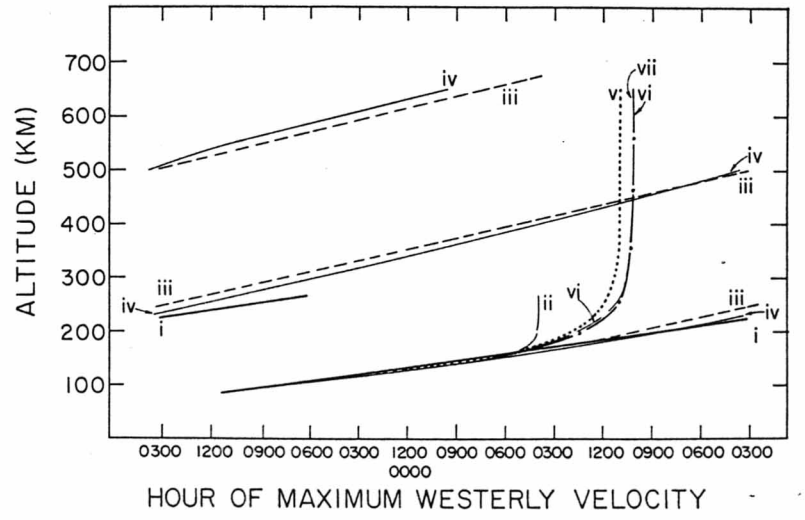

Figure 16. Same as Fig. 4—but for the second semidiurnal mode.

c

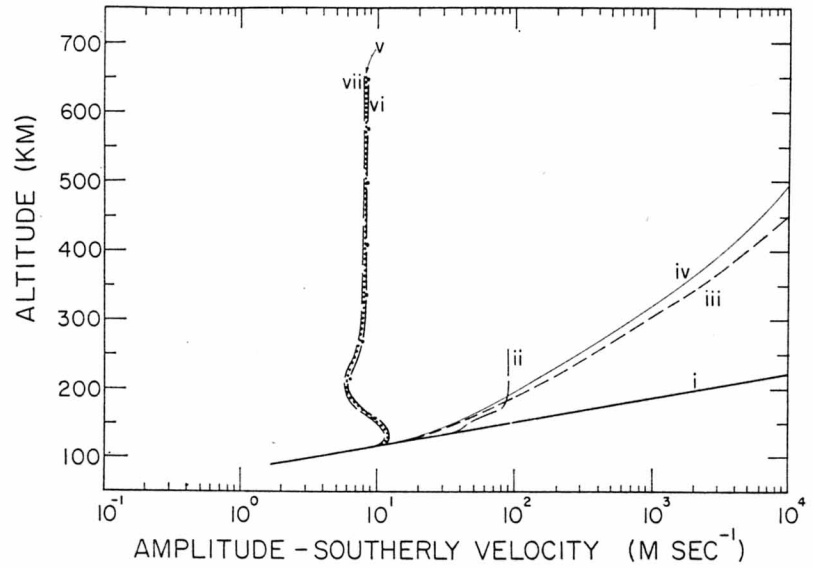

Figure 17. Same as Fig. 5—but for the second semidiurnal mode.

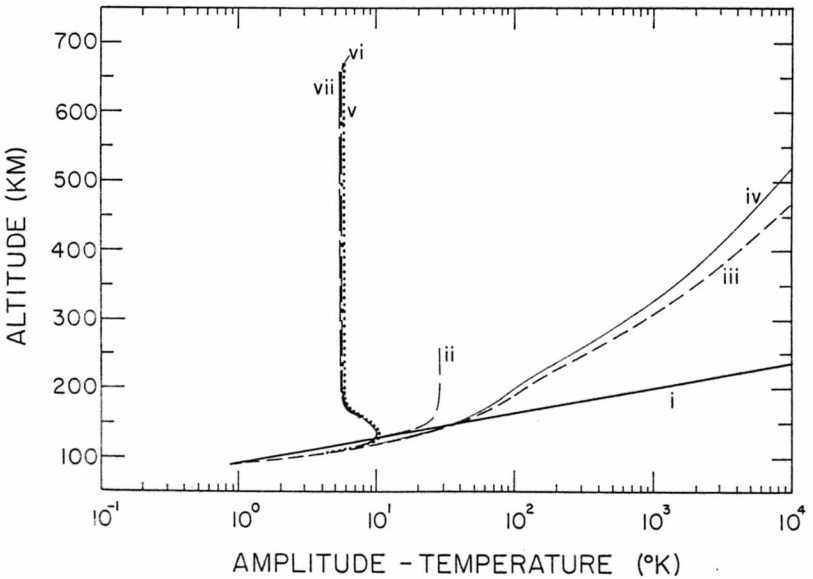

Figure 18. Same as Fig. 6—but for the second semidiurnal mode.

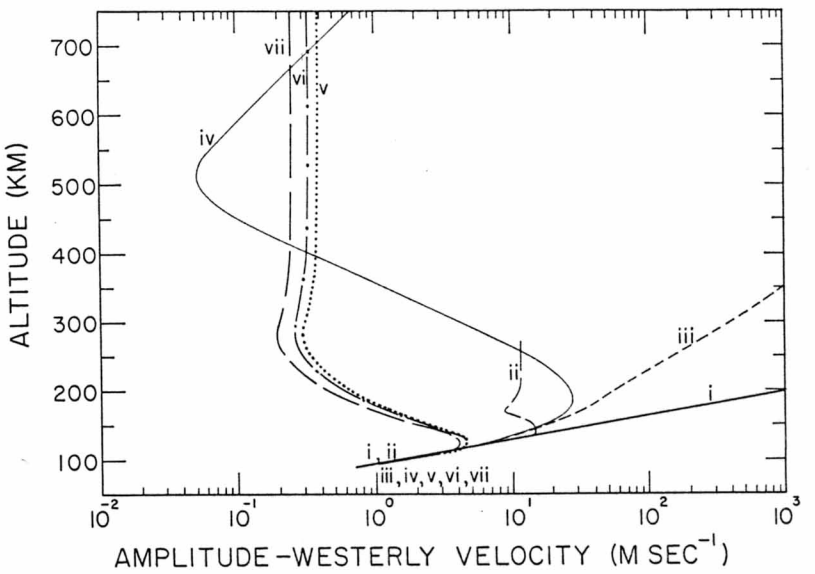

Figure 19. Same as Fig. 3—but for the 3-hour mode.

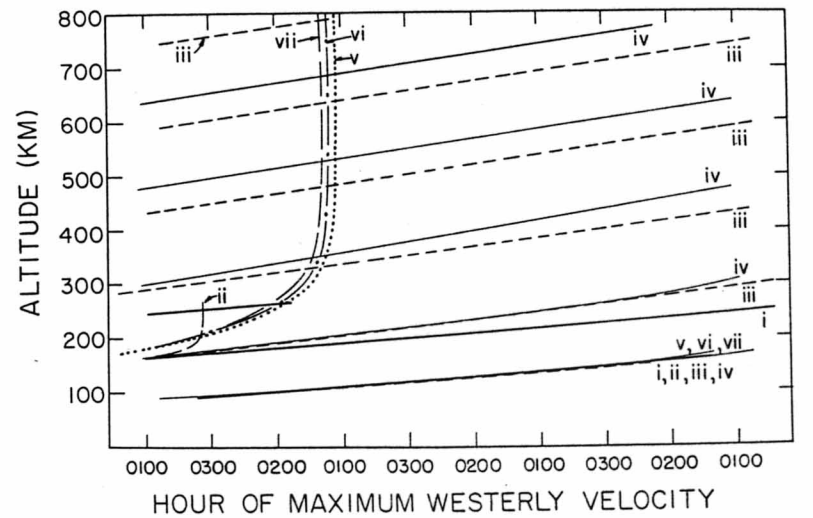

Figure 20. Same as Fig. 4—but for the 3-hour mode.

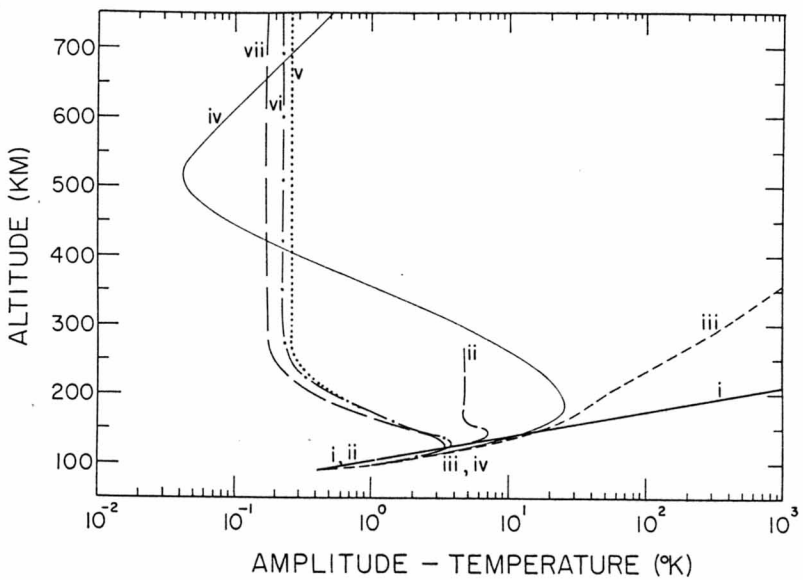

Figure 21. Same as Fig. 6—but for the 3-hour mode.

3-hr wave. We show only the phase of u' because the phases of other fields behave in a qualitatively similar manner. However, the various fields do have characteristic phase differences which vary from altitude region to altitude region. Also, the phases of different fields respond to ion drag in different ways. We, therefore, show in Table 2 the phases of u', v', T', w' and $\delta\rho'$, for models (v) and (vi), for each of the waves studied, at selected altitudes.† Also shown in Table 2 are the amplitudes of w' and $\delta\rho'/\rho_0$ at the same selected

† The phases in Table 2 are given in degrees. They may also be given in terms of the time of maximum. For diurnal oscillations

$$t_{\max} = T_1 - \frac{12\text{ hr}}{180^\circ}\,\phi. \tag{96a}$$

For semidiurnal oscillations

$$t_{\max} = T_2 - \frac{6\text{ hr}}{180^\circ}\,\phi. \tag{96b}$$

For 3-hour oscillations

$$t_{\max} = T_3 - \frac{1.5\text{ hr}}{180^\circ}\,\phi, \tag{96c}$$

where ϕ = phase in degrees and T_1, T_2, T_3 are constant determined by the known phase of the excitation.

Table 2a Diurnal Propagating Mode

Table 2 The Phases (in degrees) in Models (v) and (vi) of u', v', T', w' and $\delta\rho'/\rho_0$ for Each Mode at Selected Heights. Also shown are the amplitudes of w' and $\delta\rho'/\rho_0$.

Altitude (km)	Model (v) Phase (deg) u'	v'	T'	w'	$\delta\rho'/\rho_0$	AMP w' (m/s)	AMP $\delta\rho'/\rho_0$	Model (vi) Phase (deg) u'	v'	T'	w'	$\delta\rho'/\rho_0$	AMP w' (m/s)	AMP $\delta\rho'/\rho_0$
90	2	92	260	177	107	7.9×10^{-3}	9.2×10^{-3}	2	92	260	177	107	7.9×10^{-3}	9.2×10^{-3}
100	180	270	81	354	284	1.7×10^{-2}	1.7×10^{-2}	180	270	81	354	284	1.7×10^{-2}	1.7×10^{-2}
110	327	57	229	134	71	2.2×10^{-2}	1.9×10^{-2}	328	57	229	134	71	2.2×10^{-2}	1.9×10^{-2}
120	109	199	11	268	214	2.2×10^{-2}	1.3×10^{-2}	111	199	11	268	214	2.2×10^{-2}	1.3×10^{-2}
130	198	288	99	352	304	1.9×10^{-2}	9.0×10^{-3}	201	288	99	352	304	1.9×10^{-2}	9.0×10^{-3}
150	317	47	214	104	64	1.6×10^{-2}	4.5×10^{-3}	322	47	214	104	64	1.6×10^{-2}	4.5×10^{-3}
170	39	129	291	184	151	1.5×10^{-2}	2.6×10^{-3}	45	129	291	184	150	1.5×10^{-2}	2.6×10^{-3}
200	125	215	2	261	235	1.7×10^{-2}	1.8×10^{-3}	138	215	1	260	235	1.7×10^{-2}	1.8×10^{-3}
250	193	283	35	302	313	2.2×10^{-2}	1.7×10^{-3}	221	282	34	301	312	2.1×10^{-2}	1.7×10^{-3}
300	213	303	41	315	358	2.3×10^{-2}	2.7×10^{-3}	242	302	41	314	357	2.3×10^{-2}	2.7×10^{-3}
350	218	308	43	320	14	2.3×10^{-2}	4.0×10^{-3}	248	307	42	320	13	2.3×10^{-2}	4.0×10^{-3}
400	220	310	43	323	21	2.2×10^{-2}	5.3×10^{-3}	250	309	42	323	20	2.2×10^{-2}	5.3×10^{-3}
500	221	311	43	329	28	1.65×10^{-2}	7.7×10^{-3}	251	310	42	329	27	1.6×10^{-2}	7.7×10^{-3}
600	221	311	43	343	32	9.5×10^{-3}	1.0×10^{-2}	251	310	42	343	31	9.4×10^{-3}	1.0×10^{-2}

Table 2b Diurnal Trapped Mode

ALTITUDE (km)	MODEL (v) Phase (deg) u'	v'	T'	w'	$\delta\rho'/\rho_0$	AMP w' (m/s)	$\delta\rho'/\rho_0$	MODEL (vi) Phase (deg) u'	v'	T'	w'	$\delta\rho'/\rho_0$	AMP w' (m/s)	$\delta\rho'/\rho_0$
90	190	280	190	100	10	9.2×10^{-6}	2.0×10^{-5}	190	280	190	100	10	9.2×10^{-6}	2.0×10^{-5}
100	190	280	190	100	10	7.3×10^{-6}	1.3×10^{-5}	190	280	190	100	10	7.3×10^{-6}	1.3×10^{-5}
110	190	280	190	100	10	5.8×10^{-6}	7.7×10^{-6}	191	280	190	100	10	5.7×10^{-6}	7.7×10^{-6}
120	190	280	190	100	10	4.4×10^{-6}	4.6×10^{-6}	192	280	189	99	10	4.4×10^{-6}	4.6×10^{-6}
130	189	279	190	100	10	3.6×10^{-6}	3.1×10^{-6}	195	280	189	99	10	3.6×10^{-6}	3.1×10^{-6}
150	188	278	186	100	10	2.3×10^{-6}	1.5×10^{-6}	205	282	186	100	12	2.4×10^{-6}	1.5×10^{-6}
170	188	278	170	103	10	1.5×10^{-6}	7.7×10^{-7}	220	284	171	107	15	1.5×10^{-6}	7.4×10^{-6}
200	178	268	146	134	33	6.3×10^{-7}	3.4×10^{-7}	262	286	145	150	44	6.7×10^{-7}	3.3×10^{-7}
230	137	227	137	195	82	7.2×10^{-7}	3.4×10^{-7}	330	193	135	203	89	9.3×10^{-7}	3.8×10^{-7}
250	101	191	135	210	100	1.1×10^{-6}	4.6×10^{-7}	349	120	133	213	104	1.3×10^{-6}	5.1×10^{-7}
300	72	162	133	219	117	2.1×10^{-6}	8.4×10^{-7}	4	118	131	220	117	2.4×10^{-6}	8.9×10^{-7}
350	67	157	133	221	122	3.4×10^{-6}	1.2×10^{-6}	7	118	131	221	121	3.7×10^{-6}	1.2×10^{-6}
400	66	156	133	221	124	4.6×10^{-6}	1.5×10^{-6}	8	118	131	221	123	5.0×10^{-6}	1.5×10^{-6}
500	65	155	133	222	127	6.9×10^{-6}	2.1×10^{-6}	8	118	131	221	125	7.2×10^{-6}	2.1×10^{-6}
600	65	155	133	222	128	8.6×10^{-6}	2.6×10^{-6}	8	118	131	221	126	8.9×10^{-6}	2.7×10^{-6}

Table 2c 1st Semidiurnal Mode

ALTITUDE (km)	MODEL (v) Phase (deg) u'	v'	T'	w'	$\delta\rho'/\rho_0$	AMP w' (m/s)	$\delta\rho'/\rho_0$	MODEL (vi) Phase (deg) u'	v'	T'	w'	$\delta\rho'/\rho_0$	AMP w' (m/s)	$\delta\rho'/\rho_0$
90	28	118	253	225	192	5.8×10^{-3}	1.0×10^{-2}	29	119	254	222	192	5.9×10^{-3}	1.0×10^{-2}
100	54	144	293	239	205	1.7×10^{-2}	1.5×10^{-2}	56	145	292	237	205	1.8×10^{-2}	1.5×10^{-2}
110	88	178	328	264	227	4.0×10^{-2}	2.2×10^{-2}	88	178	326	263	229	4.0×10^{-2}	2.3×10^{-2}
120	125	215	5	298	258	7.8×10^{-2}	3.6×10^{-2}	124	213	4	299	258	7.9×10^{-2}	3.5×10^{-2}
130	158	248	43	332	288	1.2×10^{-1}	4.9×10^{-2}	159	245	44	334	287	1.2×10^{-1}	5.1×10^{-2}
150	219	309	117	35	347	2.1×10^{-1}	7.0×10^{-2}	226	307	113	32	344	2.2×10^{-1}	7.0×10^{-2}
170	279	9	164	78	34	3.3×10^{-1}	6.7×10^{-2}	290	4	154	73	33	3.2×10^{-1}	6.5×10^{-2}
200	340	70	190	113	99	4.5×10^{-1}	5.8×10^{-2}	353	55	177	108	94	3.9×10^{-1}	6.3×10^{-2}
250	14	104	203	146	156	4.2×10^{-1}	9.8×10^{-2}	30	84	187	146	142	3.7×10^{-1}	1.0×10^{-1}
300	23	113	205	184	176	3.6×10^{-1}	1.6×10^{-1}	40	92	190	186	160	3.9×10^{-1}	1.6×10^{-1}
350	26	116	206	226	184	4.4×10^{-1}	2.1×10^{-1}	43	95	190	217	167	5.3×10^{-1}	2.1×10^{-1}
400	27	117	206	251	189	6.7×10^{-1}	2.2×10^{-1}	44	96	190	236	172	7.6×10^{-1}	2.5×10^{-1}
500	27	117	206	271	193	1.25	3.6×10^{-1}	44	96	190	253	177	1.3	3.4×10^{-1}
600	27	117	206	279	196	1.8	4.5×10^{-1}	44	96	190	261	179	1.8	4.2×10^{-1}

Table 2d 2nd Semidiurnal Mode

ALTITUDE (km)	MODEL (v)							MODEL (vi)						
	Phase (deg)					AMP		Phase (deg)					AMP	
	u'	v'	T'	w'	$\delta\rho'/\rho_0$	w' (m/s)	$\delta\rho'/\rho_0$	u'	v'	T'	w'	$\delta\rho'/\rho_0$	w' (m/s)	$\delta\rho'/\rho_0$
90	132	222	19	305	253	8.2×10^{-3}	5.2×10^{-3}	132	222	19	305	253	8.2×10^{-3}	5.2×10^{-3}
100	219	309	113	36	336	2.1×10^{-2}	1.1×10^{-2}	220	309	113	36	336	2.1×10^{-2}	1.1×10^{-2}
110	308	38	205	125	60	4.4×10^{-2}	1.9×10^{-2}	309	38	205	125	60	4.4×10^{-2}	1.9×10^{-2}
120	45	135	303	216	154	7.4×10^{-2}	2.8×10^{-2}	46	135	303	216	154	7.4×10^{-2}	2.8×10^{-2}
130	118	208	17	283	228	9.1×10^{-2}	3.0×10^{-2}	120	208	16	283	228	9.1×10^{-2}	3.0×10^{-2}
150	226	316	121	20	335	1.1×10^{-1}	2.3×10^{-2}	231	315	121	20	335	1.0×10^{-1}	2.3×10^{-2}
170	302	32	195	95	56	1.1×10^{-1}	1.7×10^{-2}	309	31	194	95	55	1.1×10^{-1}	1.7×10^{-2}
200	25	115	259	166	134	1.4×10^{-1}	1.2×10^{-2}	39	114	257	164	133	1.4×10^{-1}	1.2×10^{-2}
250	92	182	292	206	214	1.7×10^{-1}	1.2×10^{-2}	116	179	289	205	212	1.7×10^{-1}	1.2×10^{-2}
300	111	201	298	223	256	1.7×10^{-1}	1.9×10^{-2}	137	198	295	221	254	1.7×10^{-1}	1.9×10^{-2}
350	117	207	299	233	271	1.5×10^{-1}	2.8×10^{-2}	142	203	297	233	268	1.5×10^{-1}	2.8×10^{-2}
400	119	209	300	245	279	1.3×10^{-1}	3.7×10^{-2}	144	205	297	246	276	1.3×10^{-1}	3.7×10^{-2}
500	120	210	300	300	286	8.4×10^{-2}	5.5×10^{-2}	145	206	297	299	283	8.9×10^{-2}	5.4×10^{-2}
600	120	210	300	349	289	1.3×10^{-1}	7.1×10^{-2}	145	206	297	346	286	1.4×10^{-1}	7.0×10^{-2}

Table 2e 3-Hour Mode

ALTITUDE (km)	MODEL (v)							MODEL (vi)						
	Phase (deg)					AMP		Phase (deg)					AMP	
	u'	v'	T'	w'	$\delta\rho'/\rho_0$	w' (m/s)	$\delta\rho'/\rho_0$	u'	v'	T'	w'	$\delta\rho'/\rho_0$	w' (m/s)	$\rho\delta'/\rho_0$
90	6		264	182	111	1.6×10^{-2}	2.3×10^{-3}	6		264	182	111	1.6×10^{-2}	2.3×10^{-3}
100	187		88	5	290	4.0×10^{-2}	4.9×10^{-3}	187		89	5	290	4.0×10^{-2}	4.9×10^{-3}
110	338		241	156	80	7.6×10^{-2}	7.8×10^{-3}	339		241	156	80	7.6×10^{-2}	7.8×10^{-3}
120	153		56	326	253	1.2×10^{-1}	1.1×10^{-2}	153		56	326	253	1.2×10^{-1}	1.1×10^{-2}
130	287		191	95	28	1.4×10^{-1}	1.0×10^{-2}	287		190	194	28	1.4×10^{-1}	1.0×10^{-2}
150	130		34	289	233	1.1×10^{-1}	5.7×10^{-3}	130		32	288	232	1.1×10^{-1}	5.5×10^{-3}
170	281		181	74	25	8.2×10^{-2}	2.5×10^{-3}	279		178	72	22	7.8×10^{-2}	2.4×10^{-3}
200	71		325	216	177	6.3×10^{-2}	1.0×10^{-3}	67		317	211	170	5.8×10^{-2}	9.8×10^{-4}
250	200		79	336	307	5.2×10^{-2}	5.7×10^{-4}	192		67	327	295	4.6×10^{-2}	5.2×10^{-4}
300	277		124	30	28	6.7×10^{-2}	4.8×10^{-4}	265		110	19	13	5.8×10^{-2}	4.3×10^{-4}
350	304		133	47	77	7.9×10^{-2}	6.5×10^{-4}	292		119	36	62	6.8×10^{-2}	5.7×10^{-4}
400	313		136	54	100	8.3×10^{-2}	9.7×10^{-4}	301		122	43	85	7.2×10^{-2}	8.4×10^{-4}
500	318		137	60	116	7.3×10^{-2}	1.7×10^{-3}	306		123	50	101	6.4×10^{-2}	1.4×10^{-3}
600	318		137	66	123	5.6×10^{-2}	2.4×10^{-3}	306		123	56	108	4.9×10^{-2}	2.1×10^{-3}

altitudes. Recall from Section 2H that w' and $\delta\rho'/\rho_0$ behave as

$$a+bz$$

in the thermosphere where a and b are complex constants. In the lower thermosphere a and b tend to be of comparable magnitude. Since a and b are complex such a linear function can (and usually does) have a non-zero minimum in amplitude at some level accompanied by phase variation with height in the neighborhood of this level. Also, if $\delta\rho'/\rho_0$ increases linearly with height, there will be some level above which $\delta\rho'/\rho_0 > 1$. It might appear that our solution will break down above this level. But, ignoring the fact that the physics we have adopted may be inappropriate above this level, there are important conditions under which this catastrophe is averted. Namely, if u', v' and T' approach constants, independent of height, at levels below the level where $\delta\rho'/\rho_0 \approx 1$, then our solutions for u', v' and T' will remain valid at all heights (representing, in essence, diffusive equilibrium for horizontal momentum and temperature). However, the hydrostatic equation (Eq. (4)) and the gas law (Eq. (6)) which relate pressure and density to temperature must (in the upper thermosphere) be solved in their non-linearized form. Since we know $T(=T_0+T')$, the problem of solving for p and ρ is still linear although the time variation of p and ρ will no longer be sinusoidal. These corrected calculations for p and ρ have not been performed in this part but an example will be presented in Part III. Figures (3)–(21) together with Table 2 are, for the most part, self explanatory. However, we shall discuss in detail the roles of conductivity and viscosity, and of ion drag.

5. Role of Viscosity and Conductivity

The first feature to be noted in Figs. (3)–(21) is that for a distance of 10 km or more above 90 km the distributions of amplitude and phase for viscous, conducting and for the inviscid, adiabatic models—given the same choice for $T_0(z)$—are almost identical.† This shows that eddy diffusion—as included here—is of almost no importance.

† The phase of the first semidiurnal mode in an isothermal atmosphere is an exception. The anomalous behavior results from reflection caused by molecular viscosity and conductivity which will be discussed later in this section—and in Part II.

Molecular viscosity and conductivity, both of which increase with height as $1/\rho_0$, are, however, of dominant importance at high altitudes. The present study to a large extent confirms the results of the more limited analytical investigations of Yanowitch[36] who only included molecular viscosity, and Lindzen[19] who studied the effect of Newtonian cooling where the rate coefficient increased as $1/\rho_0$. We therefore review the main conclusions of those studies, both of which dealt only with isothermal basic states. In these analytical studies there were two essential parameters:

$$x = \frac{4\pi^2}{L^2}\frac{\mu_0}{\rho_0}\frac{1}{\sigma} \qquad \text{(for Yanowitch[36])} \quad (97a)$$

or

$$x = \frac{a}{\sigma} \qquad \text{(for Lindzen[19])} \quad (97b)$$

(where $a \propto \text{const}/\rho_0$),
and

$$\beta = 2\pi H/L \qquad (98)$$

where L = vertical wavelength for the wave in an inviscid, adiabatic atmosphere (in terms of equivalent depth

$$L = 2\pi\left\{\left(\frac{\gamma-1}{\gamma}\right)\frac{1}{Hh} - \frac{1}{4H^2}\right\}^{-1/2};$$

see Sec. 21). χ relates the period of the wave to the time scale for dissipation (which decreases as $1/\rho_0$), while β relates the scale height for increase in dissipation to the vertical wavelength of the wave in the absence of dissipation. The main conclusions are:

(i) The increasing dissipation serves as an inhomogeneity in the medium which can cause downward reflection. The magnitude of the reflection is given by

$$|\mathscr{R}| = e^{-\pi\beta}. \qquad (99)$$

Only for the first semidiurnal mode, where for an isothermal atmosphere $L = 293$ km (viz Table 1), is reflectivity important. For the second semi-diurnal mode $|\mathscr{R}|$ is already $0(e^{-3})$.

(ii) For $\beta \lesssim 2$, wave amplitudes increase roughly as $e^{x/2}$ up to the vicinity of $\chi \sim 1$, asymptotically approaching a constant above this level—with little or no decrease of amplitude.

(iii) For $\beta > 2$, wave amplitudes increase roughly as $e^{x/2}$ up to the

vicinity of $\chi \sim 1$—but then decrease considerably before asymptoting to a constant.

(iv) The effects of dissipation become important when $\chi \gtrsim 1$. Hence, for a given β, the greater σ is, the greater the height at which dissipative effects set on.

(v) The dominance of dissipation is associated with the constancy of both amplitude and phase with height.

(vi) Most of the above results apply to waves which in the absence of dissipation propagate vertically. For evanescent waves, increasing dissipation causes wave amplitudes to cease decaying with height, approaching a constant instead. This is accompanied by a change of phase.

All the above are confirmed by our results for an isothermal basic state—except for one modest complication: namely, wave amplitudes, decreasing due to dissipation, reach a minimum above which they increase somewhat before asymptoting to a constant. This behavior is also found in the solution of Yanowitch[36] (Hines (personal communication) also reports finding this). This behavior appears to be due to the fact that increasing dissipation initially causes the effective value of L to increase thus causing a local decrease in the effective value of χ.

The main features for a basic state with variable T_0 (Model (v)) are summarized in Table 3, the details being found in Figs. (3)–(21) and in Table 2. The results are consistent with the isothermal results provided we take account of one very essential complication. The scale height now varies with height; hence, the effect of viscosity and conductivity depends on the effective value of β in the neighborhood of the height at which $\chi \sim 1$. For the diurnal propagating mode in an isothermal atmosphere $\beta \sim 2$ and the "exospheric" amplitude is only a little less than the maximum value. For the same mode in the variable temperature atmosphere, $\chi \sim 1$ at a level where H (and hence β) are considerably larger than they are in the isothermal atmosphere,† and the amplitude of the oscillation undergoes considerable attenuation. For the 3-hour mode (which has approximately the same vertical wavelength as the diurnal propagating mode) the height at which $\chi \sim 1$ is greater than for the diurnal mode because σ is much larger. At this height H (and β) are still larger and the 3-hour mode undergoes even more attenuation than the diurnal mode. In passing, it should be noted that our calculated behavior for the diurnal propagating mode is strikingly similar to the observed behavior described by Hines (1966).

The behavior of both semidiurnal modes is also consistent with the above discussion. The vertical wavelength of the first semidiurnal modes is so large that the effective β in the neighborhood of $\chi \sim 1$ is still less than 2—despite the increased value for H. Hence there is no amplitude attenuation for this mode even in the variable T_0 atmosphere; however, the increase in β is sufficient to almost eliminate the reflectivity due to increasing viscosity and conductivity (see Fig. 12). The second semidiurnal mode is now subject to an amplitude attenuation of about $\frac{1}{2}$.

† $\chi \sim 1$ at a lower altitude than in the isothermal atmosphere because (as shown in Fig. 1) below about 150 km, x, at a given height, is less for the variable T_0 atmosphere than for the isothermal atmosphere.

TABLE 3 Selected Features of Solutions for Models (v) and (vi), "Max" refers to the amplitude of a field at its lowest maximum. ( )ex refers to the amplitude of a field at the top of our domain.

		Ht. of Max $\lvert u' \rvert$ (km)	Max $\lvert u' \rvert \div \lvert u'$ (90 km)$\rvert$	$\lvert u'$ ex$\rvert \div$ Max $\lvert u' \rvert$	Ht. of Max $\lvert T' \rvert$ (km)	Max $\lvert T' \rvert \div \lvert T'$ (90 km)$\rvert$	$\lvert T'$ ex $\rvert \div$ Max $\lvert T' \rvert$
Diur. prop	Model (v)	107	2.45	0.154	109.5	3.12	0.17
	Model (vi)	107	2.45	0.112	109.5	3.12	0.17
Diur. tr.[1]	Model (v)	242	0.017	1.66	209	0.188	1.02
	Model (vi)	219	0.015	1.83	212	0.184	1.02
1st S.D.[2]	Model (v)	154	1.23×10	1.76	236	4.02×10	0.991
	Model (vi)	145	1.1×10	1.21	200	3.62×10	0.97
2nd S.D.	Model (v)	129	6.9	0.675	135	1.15×10	0.556
	Model (vi)	128	6.91	0.516	135	1.16×10	0.548
3-hr	Model (v)	126	6.3	0.081	128	9.5	0.067
	Model (vi)	126	6.2	0.072	128	9.44	0.058

[1] For diur. tr. replace maximum with minimum.

[2] The amplitude of u' for the 1st S.D. mode reaches a maximum at the height indicated. Above this height the amplitude goes to minimum and then rises again asymptotically approaching a constant value which is greater than the value at the first maximum.

The most significant effect of variable T_0 on the diurnal trapped mode is to increase the phase variation (for u' and v'—but not for T') associated with the transition from an evanescent mode to a constant amplitude mode dominated by viscosity and conductivity (see Fig. 8).

6. Role of Ion Drag

From Sec. 2E we see that the time scale for ion drag is approximately $\frac{1}{2}$ hr and the ion drag is distributed over a region 200 km thick. Thus, *a priori*, we might expect ion drag to be important for all the modes under consideration here. However, two important features prevent ion drag from necessarily being very important:

(i) Ion drag, in the present model, acts only in the west–east direction. Thus, it directly inhibits only u' within the region of ion drag. However, the degree of wave attenuation and the extent to which v', T', etc. are affected depends on whether $\partial u'/\partial x_{ew}$ or $\partial v'/\partial y$ is the dominant contributor to the horizontal velocity divergence. In the latter case the effect of ion drag is relatively small.

(ii) If the horizontal momentum balance is dominated by vertical viscous diffusion, then it is invalid to estimate the importance of ion drag by comparing its time scale with the wave period. Collisions between neutral molecules may transport momentum (and heat) across the region of ion drag in a time period short compared to the drag time scale.

By comparing results for models (iii) and (iv) (without viscosity or conductivity) we may investigate the first feature. From Figs. (3)–(21) and Table 2 we see that the 3-hr mode (without viscosity and conductivity) is drastically attenuated by ion drag. The effect of ion drag becomes progressively less as we go from the 3-hr mode to the 1st semidiurnal mode to the diurnal trapped mode, to the 2nd semidiurnal mode to, finally, the diurnal propagating mode. Reference to Table 1 shows that as the ratio $|m/k|$ increases, the effect of ion drag decreases. The physical reason for this is straightforward.

When $|m/k| \ll 1$, then $\partial u'/\partial x_{ew}$ dominates the horizontal velocity divergence and hence the generation of w' and in turn the generation of T'. Thus, when one attenuates u', one also attenuates T' and consequently the pressure gradients which force both u' and v'.

Therefore, v' is attenuated as well. Above the region of ion drag there is no longer a significant T' to regenerate the wave. When $|m/k| \gg 1$, $\partial u'/\partial x_{ew}$ contributes negligibly to the horizontal velocity divergence and the attenuation of u' leaves v' and T' relatively unaffected. Thus, there remains a temperature oscillation propagating upwards virtually unattenuated which sustains velocity oscillations. Above the region of ion drag T' regenerates u' to almost its unattenuated value.

The above discussion which is useful in illustrating the importance of anisotropy is nevertheless unrealistic since the second feature, molecular transport, is indeed of dominant importance. From Table 3 we see that the exospheric values of $|u'|$ are reduced by at most 33% by ion drag as described in Sec. 2C with $z_c = 350$ km. In the absence of viscosity and conductivity reductions of from 80–99.99 ... % occur, depending on the mode (see Figs. 3, 7, 11, 15 and 19). The exospheric value of T' is virtually unaffected by ion drag for the diurnal propagating, the diurnal trapped and the first and second semidiurnal modes. For the 3-hr mode ion drag produces a 12% reduction in both $|u'$ (exosphere)$|$ and $|T'$ (exosphere)$|$; this appears to be due to both the fact that $m/k = 0$ for this mode, and to the fact that ion drag becomes important at a level (200 km) below the level where viscosity and conductivity dominate this mode.† Associated with this last fact is the fact that reducing z_c to 320 km (or less for that matter) generally enhances the effects of ion drag (viz. the curves for model (vii) in Figs. 3–21). Conversely (though not shown here) increasing z_c generally diminishes the effects of ion drag. Such calculations demonstrate that the detailed specification of ion drag above about 350 km is unnecessary.

7. General Conclusions

Before ending this paper we wish to isolate a few major results.

(i) The two major dissipative mechanisms in the upper atmosphere are ion drag, and molecular viscosity and conductivity. For the

† The viscous and conductive attenuation of amplitude (as seen, for example, in the results for models (v), (vi) and (vii) in Fig. 19) occurs in a region where viscous and conductive terms are comparable with other terms in our equations. Dominance of viscosity and conductivity is associated with constancy of amplitudes and phases (see Sec. 5).

modes we have studied our results show that molecular viscosity and conductivity are far more important than ion drag. What we mean by this is the following. Let us call our solution including both ion drag and molecular viscosity and conductivity the " correct " solution. If we now omit ion drag our solution will vary from the " correct " solution by no more than about 45% in wave amplitudes —and usually much less. If, however, we retain ion drag but omit molecular viscosity and conductivity our solution will vary (in the upper atmosphere) from the " correct " solution by orders of magnitude. A study of Figs. 3–21 shows, moreover, that molecular viscosity and conductivity are of comparable importance contrary to the claims of Volland (1969).

(ii) Of the propagating modes studied, all, except the first semidiurnal mode, cease growing approximately as $e^{x/2}$ below 120 km and undergo significant amplitude attenuation before asymptoting to constant amplitudes. The first semidiurnal mode, on the other hand, continues growing as about $e^{x/2}$ until about 150 km and undergoes no amplitude attenuation. Thus, anticipating results to be discussed in Parts II and III, we find that of all the tidal modes excited in the lower atmosphere it is only the first (and main) semidiurnal mode which is efficiently transmitted to the thermosphere. From observations (see Lindzen and Chapman[20]), $|u'|$ for this mode is about 10 m/s at 90 km. From Figs. 11 and 14 we may then infer exospheric values of $|u'| \sim 134$ m/s, and $|T'| \sim 187°$— which clearly imply that this mode is of great importance in the thermosphere.

The above are the most obviously important conclusions to emerge from Part I. There is another conclusion whose full importance will become clear in Part III.

(iii) For the diurnal propagating mode the effect of viscosity and conductivity is to end $e^{x/2}$-growth and introduce substantial amplitude attenuation between about 110 km and 210 km. This effect is enhanced by ion drag (for $|u'|$ at least). For the diurnal trapped mode the effect of viscosity and conductivity is to end exponential decay of amplitude with height. Ion drag has, on the whole, very little effect on this mode. As a result of the above, the so called trapped mode is just as effective as the so called propagating mode in transmitting a disturbance from the lower to the upper thermosphere.

Moreover, for excitation distributed throughout the lower thermosphere, the trapped mode will be more efficient because it involves less phase variation with height than the propagating mode and, therefore, gives rise to less destructive interference.

Acknowledgements

Acknowledgement is due the National Science Foundation for support through grant GA-1622. Acknowledgement is also made to the National Center for Atmospheric Research, which is sponsored by the National Science Foundation, for use of its Control Data 6600 computer. Thanks are due to Mr. Paul Swartztrauber for his help in adapting our programs to CDC 6600 computer. Special thanks are due to Mrs. Donna Blake for her aid in checking equations, programming, and preparing diagrams. Finally, the hospitality of the Department of Environmental Sciences of Tel Aviv University, where this paper was written, is gratefully acknowledged.

REFERENCES

1. Carrier, G. F. and Pearson, C. E., *Ordinary Differential Equations*, Blaisdell Publishing Company, Waltham, Mass., 229 pp. (1968).
2. Cowling, T. G., " The electrical conductivity of an ionized gas in a magnetic field with application to the solar atmosphere and the ionosphere," *Proc. Roy. Soc. London, A*, **183**, 453–479 (1945).
3. Craig, R. A. and Gille, J. C., " Cooling of the thermosphere by atomic oxygen," *J. Atmos. Sci.* **26**, 205–209 (1969).
4. Dickinson, R. E. and Geller, M. A., A generalization of " Tidal theory with newtonian cooling," *J. Atmos. Sci.* **25**, 932–933 (1968).
5. Flattery, T. W., *Hough Functions*, Technical Report, No. 21, Dept. of Geophysical Sciences, University of Chicago (1967).
6. Geisler, J. E., " Atmospheric winds in the middle latitude F region," *J. Atmos. Terrest. Phys.* **28**, 703–721 (1966).
7. Harris, I. and Priester, W., " On the diurnal variation of the upper atmosphere," *J. Atmos. Sci.* **22**, 3–10 (1965).
8. Haurwitz, B., *Tidal Phenomena in the Upper Atmosphere*, W.M.O. Rept., No. 146, T.P.69 (1964).
9. Hines, C. O., " Internal gravity waves at ionospheric heights," *Canad. J. Phys.* **38**, 1441–1481 (1910).
10. Hines, C. O., " The upper atmosphere in motion," *Quart. J. Roy. Meteor. Soc.* **89**, 1–42 (1963).
11. Hines, C. O., Comments on a paper by D. G. King-Hele, *Planetary Space Sci.* **13**, 169–172 (1965).

12. Hines, C. O., " Diurnal tide in the upper atmosphere," *J. Geophys. Res.* **71,** 1453–1459 (1966).
13. Hirschfelder, J. O., Curtis, C. F. and Bird, R. B., *Molecular Theory of Gases and Liquids*, Wiley, New York, 1249 pp. (1954).
14. Hunt, B. G., " The need for a modified photochemical theory of the ozonosphere, *J. Atmos. Sci.* **23,** 88–95 (1966).
15. King, J. W. and Kohl, H., " Upper atmospheric winds and ionospheric drifts caused by neutral air pressure gradients," *Nature* **206,** 699–701 (1965).
16. Kuo, H. L., " The thermal interaction between the atmosphere and the earth and propagation of diurnal temperature waves," *J. Atmos. Sci.* **25,** 682–706 (1968).
17. Lindzen, R. S., " Reconsideration of the diurnal velocity oscillation in the thermosphere," *J. Geophys. Res.* **72,** 1951–1958 (1967).
18. Lindzen, R. S., " The application of classical atmospheric tidal theory," *Proc. Roy. Soc. London, A,* **303,** 299–316 (1968).
19. Lindzen, R. S., " Vertically propagating waves in an atmosphere with Newtonian cooling inversely proportional to density," *Canad. J. Phys.* **46,** 1835–1840 (1968a).
20. Lindzen, R. S. and Chapman, S., " Atmospheric tides and thermal tides,' *Space Sci. Rev.*, **10,** 3–188 (1969).
21. Lindzen, R. S. and Goody, R. M., " Radiative and photochemical processes in mesospheric dynamics. Part I: Models for radiative and photochemical processes," *J. Atmos. Sci.* **22,** 341–348 (1965).
22. Lindzen, R. S. and Kuo, H. L., " A reliable method for the numerical integration of a large class of ordinary and partial differential equations," *Mon. Wea. Rev.*, **97,** 732–734 (1969).
23. Martyn, D. F., " Interpretation of observed F_2 ' winds ' as ionization drifts associated with the magnetic variations," *The Physics of the Ionosphere, Rept. of the Physical Society, London,* 163–165 (1955).
24. Midgely, J. E. and Liemohn, H. B., " Gravity waves in a realistic atmosphere," *J. Geophys. Res.* **71,** 3729–3748 (1966).
25. Murgatroyd, R. J. and Goody, R. M., " Sources and sinks of radiative energy from 30 to 90 km," *Quart. J. Roy. Met. Soc.* **84,** 225–234 (1958).
26. Nicolet, M., " The properties and constitution of the upper atmosphere," in *Physics of the Upper Atmosphere*, J. A. Ratcliffe, editor, Academic Press, New York, 17–72 (1960).
27. Panofsky, H., " Internal atmospheric turbulence," *Bulletin Amer. Met. Soc.* **50,** 539–543 (1969).
28. Paulin, G., " A simplified method of computing stratospheric heating rates and associated generation of available potential energy," *Mon. Wea. Rev.* **97,** 359–370 (1969).
29. Pitteway, M. L. V. and Hines, C. O., " The viscous damping of atmospheric gravity waves," *Can. J. Phys.* **14,** 1935–1948 (1963).
30. Reed, R. J., Oard, M. J. and Sieminski Marya, " A comparison of observed and theoretical diurnal tidal motions between 30 and 60 km," *Mon. Wea. Rev.* **97,** 456–459 (1969).
31. Rodgers, C. D. and Walshaw, C. D., " The computation of infrared cooling rate in planetary atmospheres," *Quart. J. Roy. Met. Soc.* **92,** 67–92 (1966).

32. Spizzichino, A. and Revah, I., " Mouvelles donnees experimentale sur les differentes composantes du vent au moyen d'un radar meteorique," *Space Research,* **VIII,** 679–682 (1968).
33. Vincent, R. A., " A criterion for the use of the multilayer approximation in the study of acoustic gravity wave propagation," *J. Geophys. Res.* **74,** 2996–3001 (1969).
34. Volland, H., " A theory of thermospheric dynamics—I, Diurnal and solar cycle variations," *Planet. Space Sci.*, **17,** 1581 (1969).
35. Wallace, J. M. and Hartranft, F. R., " Diurnal wind variations; surface to 30 km," *Mon. Wea. Rev.* **96,** 446–455 (1969).
36. Yanowitch, M., " Effect of viscosity on gravity waves and the upper boundary condition," *J. Fluid Mech.* **29,** 209–231 (1967).